A224808

Acoustic Reflections from Cylindrical Blocks of Arctic Ice, 1988

by
G. R. Garrison
R. E. Francois
T. Wen
W. J. Felton

Technical Report
APL-UW TR 8815
January 1990

Applied Physics Laboratory University of Washington
Seattle, Washington 98105-6698

Contract N00039-88-C-0054

Approved for public release; distribution is unlimited.

ACKNOWLEDGMENTS

This research was supported by the Office of Naval Technology (ONT) with technical management provided by the Naval Oceanographic and Atmospheric Research Laboratory (NOARL). The authors appreciate the equipment support by Ronald Stein and reviews of the report by Kevin Williams and Pierre Mourad.

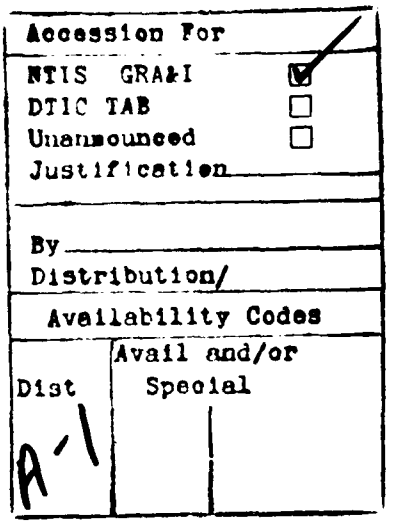

CONTENTS

LIST OF FIGURES

ABSTRACT

In spring 1988 acoustic reflections were measured from the submerged ends of cylindrical blocks of arctic ice, in an extension of similar efforts in 1984 and 1986. Blocks with diameters of 27, 38, 58, and 84 cm were individually depressed below the surface of the ice floe so that reflections from the bottoms of the blocks were separable from those off the underside of the ice canopy. The source/receiver was moved horizontally beneath the block to measure the angular response pattern. Measurements to determine the effect of the so-called skeletal layer showed that compared with solid ice the layer reduced the reflection at normal incidence by 8–11 dB in the frequency range 20–80 kHz for all blocks. Properties of the skeletal layer and the transition zone were also measured to study the nature of the reflection.

I. EXECUTIVE SUMMARY

To operate effectively in arctic regions, the acoustic systems of submarines and underwater weapons must take into account the physical and acoustic characteristics of the ice-covered seas. Movement of the ice produces cracking and ridging, resulting in ice keels that are an important source of interference for acoustic navigation systems or weapons. Performance could be greatly improved by developing more accurate acoustic models of ice keel reflections.

Ice keel reflections appear to result from a small number of discrete scatterers rather than being a reverberationlike sum that can be treated statistically. Thus most models are based on a random orientation of blocks with each face assigned a target strength depending on size and aspect. To obtain empirical data on the target strength of such faces, the Applied Physics Laboratory conducted field experiments in 1984 and 1986[1,2] in which reflections were measured from the end of a cylindrical block that was cut from the ice cover and depressed below the surrounding ice. The spring 1988 experiment reported here is a continuation of that study.

The measured reflections are much smaller than those predicted for a flat water-ice interface with its large change in acoustic impedance. It is apparent that the skeletal layer formed as the ice freezes considerably reduces reflection at normal incidence, especially at the high end of the 20–80 kHz frequency range used in the study. The skeletal layer (defined here as the outer few centimeters of growing sea ice) and the transition zone above contain brine that has been displaced by the freezing process and sandwiched between vertically oriented platelets of pure ice. This gradual transition from a fluid to a solid state reflects less sound than does solid ice.

The spring 1988 measurements allow comparisons between normal-incidence reflections from the skeletal layer, from an air-water interface, and from solid ice. The measurements involved five frequencies (20–80 kHz) and blocks of four diameters (27–84 cm). The results are summarized as follows:

1. The water-ice interface of flat first-year ice, with its skeletal layer, produced a reflection response pattern with the general shape predicted for an air-water interface, but the peaks and nulls were usually somewhat smoothed. The target strength varied in accord with theory for the four differently sized blocks but was 8–11 dB lower than that measured for solid ice.

2. The corresponding amplitude reflection coefficient for the skeletal surface at normal incidence decreased gradually from 0.20 to 0.12 as the frequency increased from 20 to 80 kHz. The decrease was greater at the higher frequencies, where the size of surface irregularities becomes appreciable with respect to acoustic wavelength.

3. Removal of the blocks from their original environment produced the following changes in reflectivity which provide clues about the nature of the skeletal layer and transition zone:

    (a) The reflectivity decreased following submergence of a block; this is probably related to the change in temperature, and therefore sound speed, caused by warming of the block by the surrounding water.

    (b) The reflectivity increased after a block had been raised, insulated, drained, and relowered. A 180° phase change indicated the increase was caused by trapped air.

    (c) The reflectivity increased after a block had been removed and cooled, probably owing to freezing of the skeletal layer and transition zone into a more solid structure.

4. Tests with four circular water-air interfaces about the same size as the ice blocks showed a stable acoustic reflection with a directional response pattern in excellent agreement with that predicted using Huygens' principle for a rigid flat plate. The pattern includes several side lobes. The close agreement with theory verifies that the air surfaces make good calibration targets.

These results confirm that the effect of the skeletal layer must be included in future modeling efforts.

II. INTRODUCTION

Ice ridges are formed when pressure causes the ice to crack and pile up into masses of crushed and broken ice blocks as shown in Figure 1. In measuring the acoustic reflections from the corresponding keels projecting into the water below, it is not clear what configuration of blocks produces reflections, which are observed to be individual and sporadically spaced along the keel. A slab of ice that has been forced downward and tilted into a vertical position nearly normal to the incident sound beam would be a likely source of the largest reflections.

Measurements were performed in the fall of 1984,[1] the spring of 1986,[2] and the spring of 1988 to study reflection at normal incidence from faces of first-year ice containing the natural skeletal layer formed during freezing. Such a face, because it is relatively flat and usually larger than the other faces, may be a major keel reflector; therefore the amplitude, response pattern, and seasonal nature of its reflection are important factors in predicting the acoustic response of ice keels.

Figure 1. A typical pressure ridge formed in ice 40 cm thick.

In the two earlier experiments, the variability in the reflectivity of different diameter blocks taken from first-year ice indicated that the lower faces of the blocks were not flat. In the present experiment, the flatness of the lower face of the blocks was measured directly. A small, reflective sphere placed near the ice block provided a continual check on equipment performance. Circular, air-filled metal pans, one for each sized block, provided accurate calibration of the reflections. Measurements on a block with the lower surface removed allowed a comparison of reflections from solid ice and from ice with a skeletal layer. Supporting measurements were made of the flatness of the under-ice surface and of the temperature and salinity profiles in the ice to help understand the nature of the skeletal layer reflection.

The experiment was conducted the last week of March 1988 at ice camp APLIS in the Beaufort Sea as part of ICEX-88, one of a series of on-going experiments by the U.S. Navy. The schedule of events is given in Table 1. A large refrozen lead, 1.4 m thick, was selected for the experiment because it appeared very flat and uniform. Four cylindrical blocks with diameters of 27, 38, 58, and 84 cm were cored out with an APL thermal drill, which forces hot water through small holes in a circular manifold to melt a 5-cm wide circular groove in the ice. When free, each block was forced down 1 m and guyed into a fixed position with the lower face horizontal. Reflections were measured and the block was removed. The 58-in. block was reinstalled three times—once after draining, once with the top sawed off, and once with the top and bottom sawed off. A similar block was sawed off on both ends after lying exposed on top of the lead for 4 days. The air temperature was considerably lower than the water temperature; thus the time that the blocks resided in the air or beneath the surface would have affected their temperature at the time of the measurement. The environmental conditions are described in Ref. 3. A cross-sectional view of the various blocks measured, including the reference targets, is shown in Figure 2.

A transducer suspended 27 m below the block transmitted sound pulses and received the reflections from the lower face of the block. The transducer was suspended on three lines so that it could be moved along a path beneath the block. These support lines were installed from above by passing a lightweight line through drilled holes spaced 2–3 m apart rather than being installed by divers as in the earlier experiments, because the divers left an accumulation of air beneath the surface.

Table I. Schedule of events.

Date	Time	Event
18 March	a.m.	Selected a flat site. Surveyed locations of blocks, pipes, frame, and poles.
	p.m.	Installed frame and poles.
19 March	a.m.	Tried out line-passer as a means of stringing a line under the ice from hole to hole.
	p.m.	Moved an 8 × 8 ft hut to the ice block site.
20 March	a.m.	Drilled a string of holes at 2-m spacing for line passing.
22 March		Completed line passing.
24 March		Suspended a 20-cm diameter sphere 30 cm south of center at a depth of 6 m.
25 March		Took an ice core at the site.
26 March		Measured some one-way transmissions through the ice (a separate experiment). Tested transducers.
27 March	a.m.	Made some under-ice surface reflection measurements in the vicinity of the planned ice blocks (a separate experiment).
	p.m.	Cored and positioned 38-cm block. Measured reflections along two cross lines, Run 1.[a]
28 March	a.m.	Cored and positioned 27-cm block. Removed 38-cm block and measured flatness.
	p.m.	Measured reflections from 27-cm block, Run 2. Noticed interference later found to be from the cable used in a neighboring operation.
29 March	a.m.	Cored and positioned 84-cm block. Measured reflections, Run 3.
	p.m.	TV inspection of block and surroundings. Cored and removed a 58-cm block for practice in handling and sawing. Measured flatness of 27-cm block.
30 March	a.m.	Identified neighboring cable as source of interference; raised cable out of range. Repeated 84-cm block measurements to investigate the time change in the reflections, Run 4.
	p.m.	Cored and positioned 58-cm block. Measured reflections, Run 5. Measured flatness of 84-cm block. Started time series on 58-cm block.
31 March	a.m.	Completed time series on 58-cm block. Measured flatness of 58-cm block. Raised 58-cm block, insulated the lower portion, and allowed it to drain for 40 min.
	p.m.	Lowered the block and measured reflections, Run 6. Removed the block and sawed off top 48 cm. Reinstalled and measured reflections, Run 7.
	p.m.	Removed block and sawed off 15 cm from the bottom. Reinstalled and measured reflections, Run 8.
1 April	a.m.	Installed 60-cm air cylinder and measured reflections, Run 9.
	p.m.	Same for 86-cm air cylinder, Run 10.
2 April	a.m.	Same for 40- and 28-cm air cylinders, Runs 11 and 13. Made Run 12 with 28-cm pan with all the air released.
	p.m.	Sawed out a 62-cm length of the practice 58-cm block (very cold, hard ice). Installed it in the largest hole and measured reflections, Run 14.
3 April	a.m.	Took second ice core at the site.
8 April		Took third and fourth cores near the site.

[a] A pair of perpendicular passes of the transducer beneath the block is called a run.

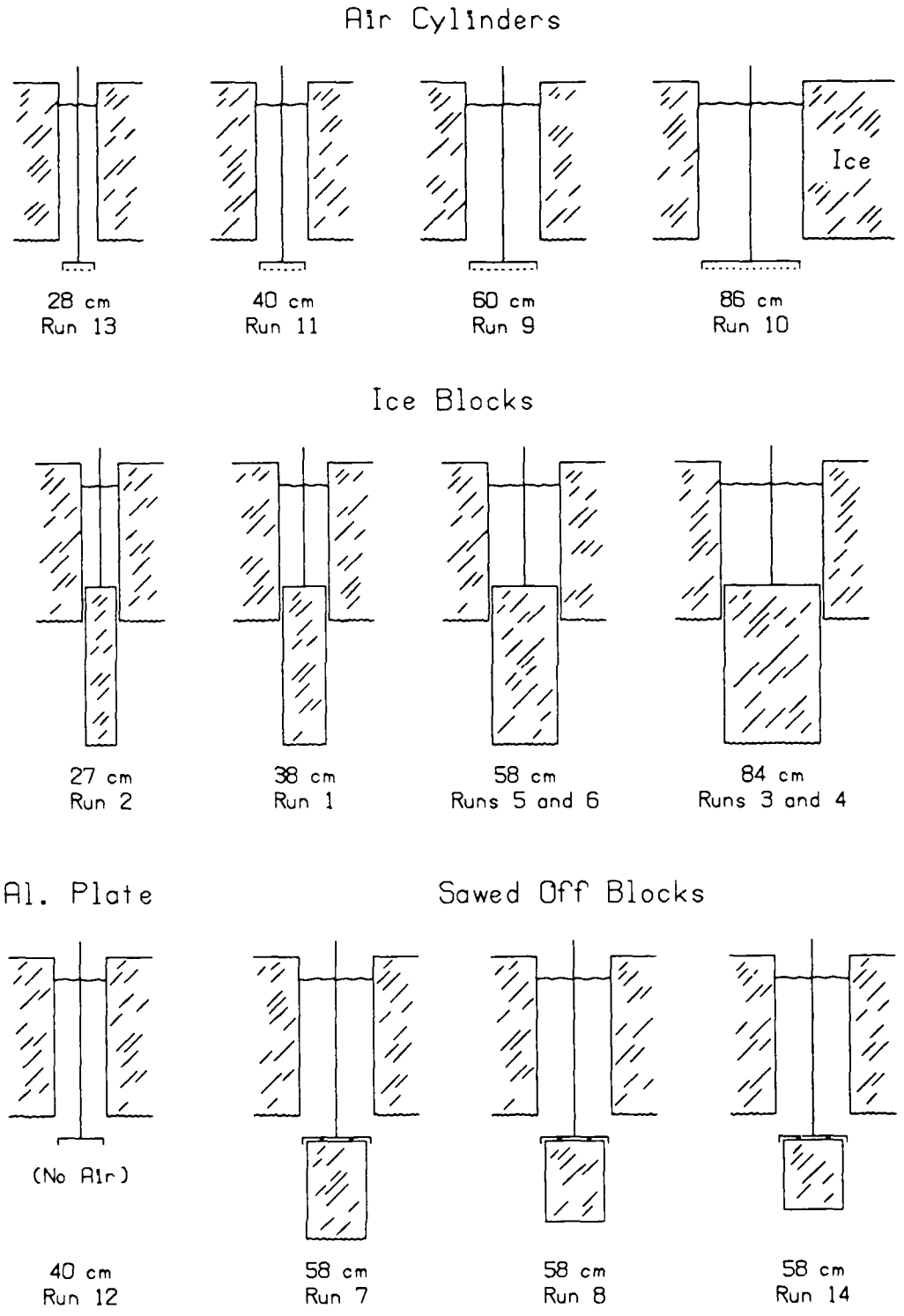

Figure 2. The various block faces measured during the ice block reflection experiment. (Drawn to scale except that the bottom roughness is greatly exaggerated.)

III. EXPERIMENTAL ARRANGEMENT

The experimental arrangement (Figures 3–8) remained the same as in 1984 and 1986.[1,2] The transducer was connected by lines to a ring, which was placed over one of many pegs on a rectangular wooden frame so that the position of the transducer could be calculated from the position of the ring. The spacing of the pegs was 15 cm, and the corresponding movement of the transducer below was about 21 cm. The accuracy of the positioning is estimated to be 10 cm. Each peg was labeled by its north (N) and east (E) coordinates. After determining the coordinates for which the transducer output was maximum, we made two perpendicular passes through that position, one north south and one east-west.

In preparation for the experiment, the locations of the blocks, the frame, and the support lines were carefully surveyed. At the location planned for each block, a 30-cm deep, 10-cm diameter hole was drilled in the ice. A 3-m long, 5-cm diameter aluminum pole was then plumbed vertically in the hole, and fresh water and snow were packed around the pole. By the next day, the poles were frozen solidly in place. After each block was cut out and pushed down into position, guys were adjusted to keep the pole vertical and thus ensure that the lower face of the block was horizontal, or at least as nearly so as it was originally.

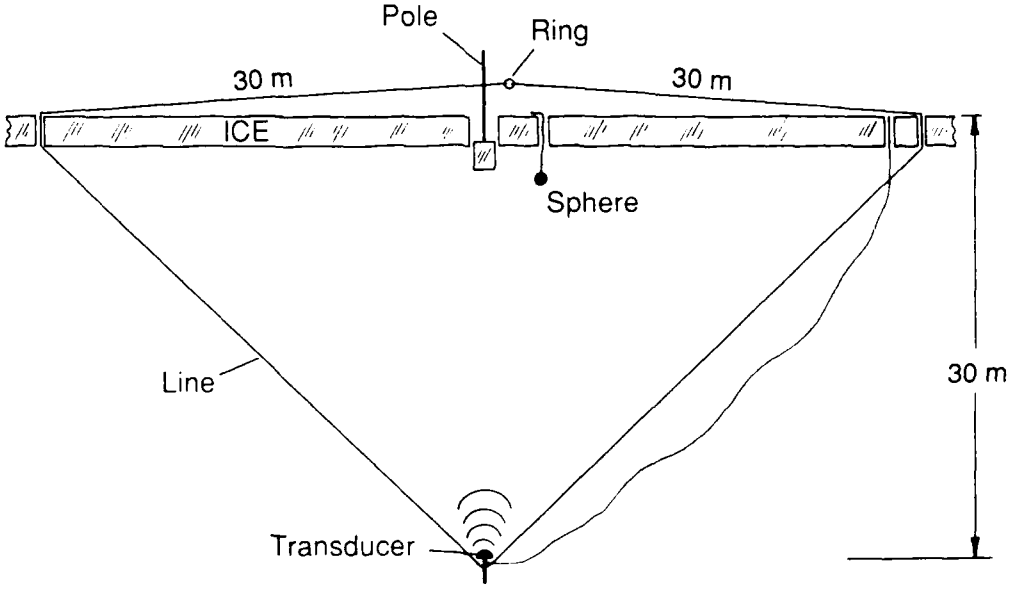

Figure 3. Experimental arrangement for ice block experiment, elevation view for a two-dimensional simplification.

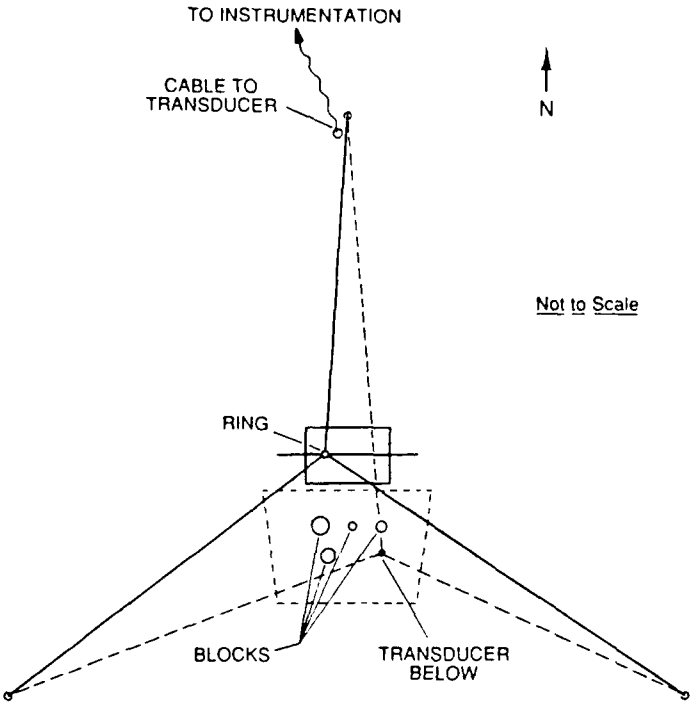

Figure 4. Experimental arrangement, plan view. Movement of the ring on the frame gives a somewhat greater movement of the transducer below.

Figure 5. A 5-cm ring, to which three lines are hooked, is placed over one of the pegs.

Figure 6. Attaching wires to hold the pole vertical after the block has been pushed down.

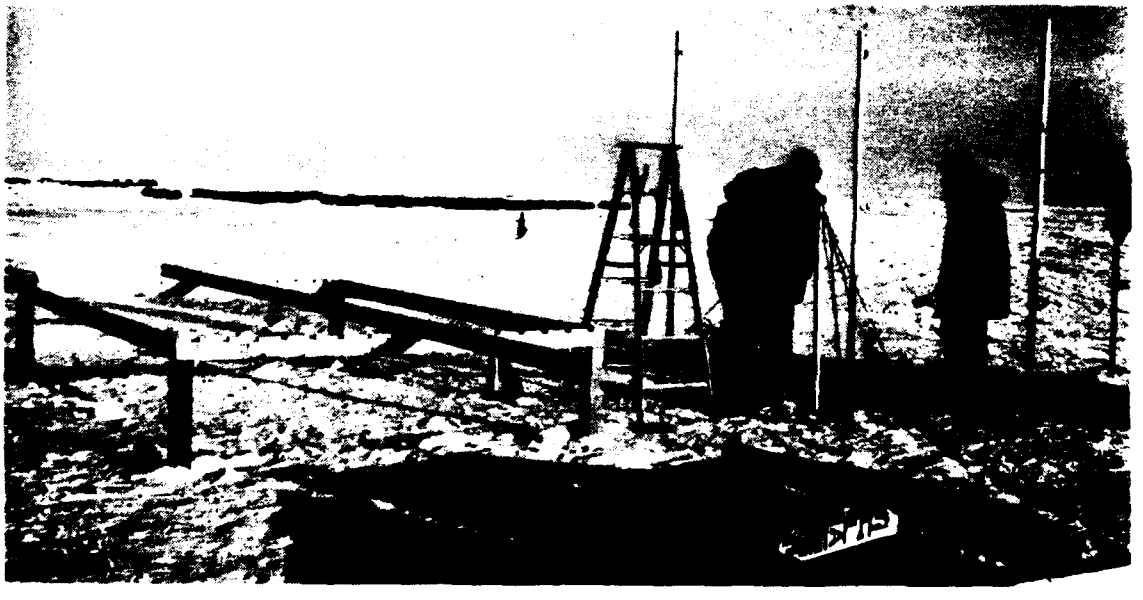

Figure 7. A block with protruding pole has been cored out and pushed down into position.

Figure 8. Equipment in operation during the ice block experiment. At the left, the coring ring has been placed around a pole in preparation for attaching the hot-water hoses. At the center, a block used for the previous measurement is ready to be removed.

For transducer entry, a 90-cm diameter hole was cored with the APL thermal drill (Figure 9) near the position of one of the support-line holes. After the three 23-cm holes for the support lines were made, a series of holes was drilled along lines between the entry hole and the two remote support-line holes. A recently designed "line-passer" was used to transfer lines beneath the ice from the transducer entry to the adjacent support-line hole and to each of the other support-line holes. To keep the line from rubbing on the edge of the hole, it was run through a 5-cm diameter plastic pipe about 2 m long. When all three lines were connected to the transducer, it was lowered into position. The first block was melted out, forced down, and secured with wooden wedges. The pole was held vertical with three lines. After the reflections were measured from that block, the procedure was repeated for the other blocks.

The transmitting, receiving, and recording equipment was operated in a plywood building 100 m from the measurement site. For the experiment, 0.5-ms cw pulses at five

Figure 9. The APL thermal drill in the process of coring an ice block.

frequencies in the interval 20–80 kHz were transmitted from the transducer, and the envelopes of the returns were recorded on a Nicolet digital oscilloscope. Prior to each reflection run, the transmit pulses and the raw return at normal incidence were recorded on a Nicolet diskette for later analysis. In addition, the envelopes of the signals were recorded on a video cassette recorder as a backup.

The transducer used throughout the experiment was an ITC 1042. Its characteristics over the frequency range 20–80 kHz (Figure 10) were measured at the APL acoustic calibration barge in Seattle's Lake Union. The temperature of the lake water was much higher than that in the Arctic, and the acoustic response of the transducer has a strong temperature dependence. The frequency response curves measured at the barge give roughly the variation with frequency but are not suitable for arctic conditions. A method of calibration in the field is described in the next section.

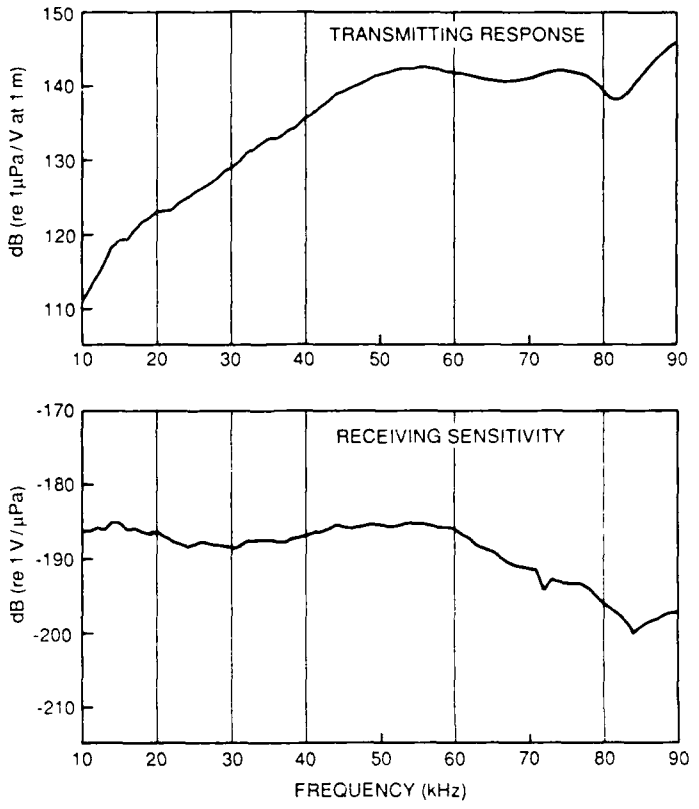

Figure 10. Frequency response of the ITC 1042 transducer as measured at the APL acoustic calibration barge.

IV. FIELD CALIBRATION

A sphere of known target strength was placed at slightly shorter range than the reflectors, so that its return was present in every ping. Arriving prior to the ice block return, it caused no interference and provided a good calibration check on the equipment.

For greater accuracy, we also used a flat air-water interface of known area for calibration. We obtained this surface by submerging an inverted metal pan and filling it with air through a hose from the surface (see Figure 11). The calibration was performed after completing the acoustic measurements of all the blocks to avoid contaminating the under-ice area with vented air. We attached a pole to the pan and pushed it down through the 84-cm hole. When it was in the position previously occupied by the block, we added air to provide a flat, level air-water interface. We then measured its reflection, keeping all equipment parameters the same as when measuring the ice block reflections. Four separate pans were used to match the size of each ice block measured.

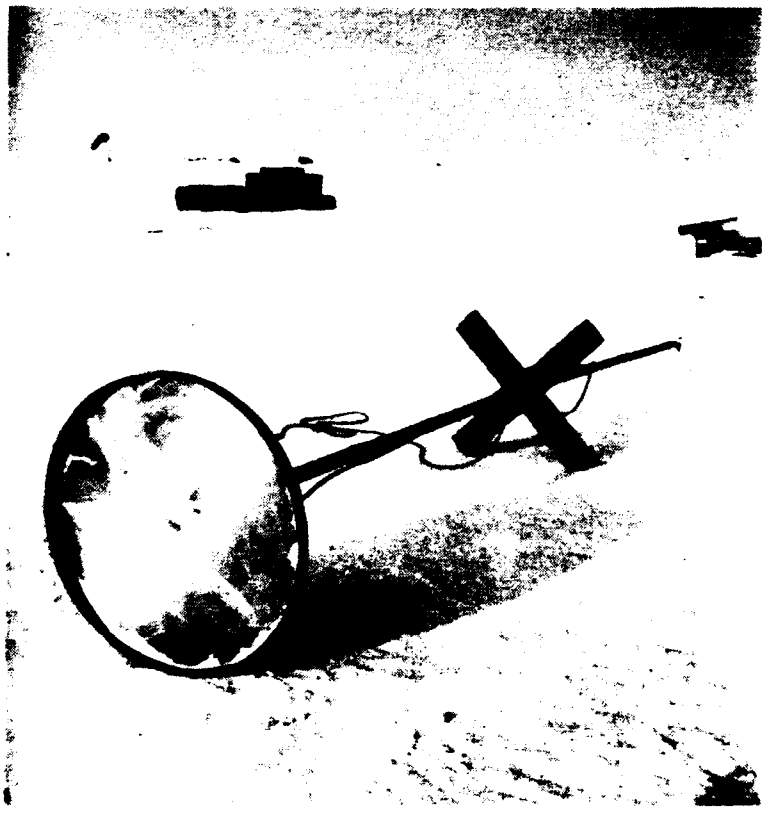

Figure 11. Pan that forms an air-water interface when lowered with the open face downward and filled with air through the attached hose.

A. Air Block Returns

The pressure relief surface provided by an air-water interface produces a large impedance mismatch; therefore the target strength given by Urick[4] for a flat rigid circular plate is applicable, assuming that the surface has an amplitude reflection coefficient of unity.

$$TS = 20 \log [(\pi a^2/\lambda)\, 2 J_1(\beta)/\beta \cos\theta] \quad [\text{dB}] , \tag{1}$$

where

a = radius of plate

λ = wavelength

J_1 = Bessel Function

θ = incident angle

$\beta = 4\pi a/\lambda \sin\theta$.

The equation is good in the far field, i.e., for range >> a^2/λ. To correct for the slightly near-field conditions for the 84-cm block, we also calculated the return by numerically integrating over the surface, assuming each incremental area to act as a source with a strength proportional to the log of the area. All contributions were added, using Huygens' principle and taking into account the phase difference caused by differences in range. The exact method is described in Ref. 2. The numerical integration gave the same results as Eq. 1 at long ranges and therefore was considered accurate at the slightly near-field ranges of this experiment. All theoretical response patterns shown in this report represent near-field patterns appropriate to the geometry.

As an auxiliary test, we removed the air from an inverted pan and measured the returns from the 3.2-mm thick metal surface of the pan by the method described in the next section. The results are shown in Figure 12, in which the theoretical curves from Eq. 1 have been added for comparison. The reflectivity does not drop off with frequency as it does for an ice surface. The target strength is nearly as great at the higher frequencies as at the lower frequencies. During calibration, when the pan was filled with air, the sound should not have reached the metal surface of the pan; therefore reflections from the pan itself should not be involved.

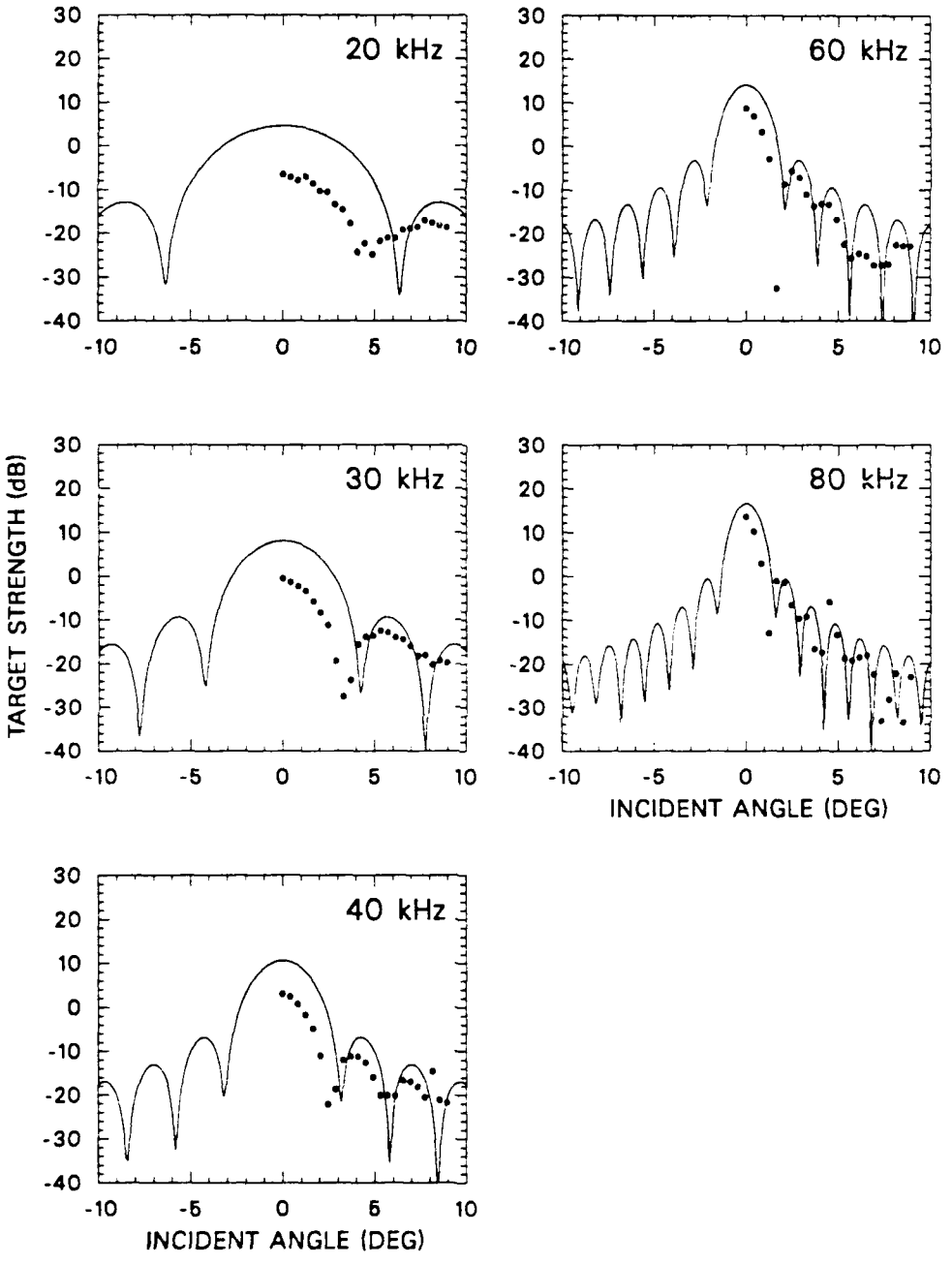

Figure 12. Reflections from a water-filled 40-cm diameter aluminum pan that was previously filled with air for calibration purposes. The theoretical pattern (Eq. 1, solid line) is shown for comparison.

The response patterns for the air-filled pans were obtained by the procedure described in Section V. They are plotted in Figures 13–20, where we have adjusted the transducer calibration constants at each frequency to give the best fit of the measurements at all four block sizes to the theoretical curves for a rigid circular plate. The points fit the pattern remarkably well for all four sizes of blocks, showing that the experimental method is accurate and that the theory is appropriate.

In these target strength calculations, it is not necessary to know the receiving sensitivity and transmitting response of the ITC 1042 transducer individually. Instead, we use only the sum. The sums derived for the air block reflections were −75, −70, −65, −50 and −50 dB for 20, 30, 40, 60, and 80 kHz, respectively.

B. Sphere Returns

A 20-cm diameter, stainless steel sphere filled with Freon TF fluid was placed in the field of view of the transducer for the duration of the experiment. (Freon increases the target strength by focusing the incoming sound onto the back face of the sphere.) The sphere's reflection arrived 5 ms before the ice block's reflection and was readable in every ping.

Examples of the target strength of the sphere as the transducer moved along a path beneath an ice block are shown in Figures 21 and 22. The transducer did not pass directly under the sphere, and thus there is a gap in the readings for incident angles near zero (vertical transmission).

Figure 21 shows a broad dip in the return at some angles below the sphere at the higher frequencies. This anomaly is noticeable at 60 kHz and quite pronounced at 80 kHz. At first it was thought to result from modifications made to the back side of the sphere to install a filling port and a connector for the support line. However, a disturbance to the back face would be expected to cause an anomaly when the transducer was directly below the sphere. No such anomaly appears in Figure 22 for a run in which the transducer passed almost directly beneath the sphere. After returning to Seattle, we hung the sphere on a line in still water and passed the transducer beneath it to look for this anomaly. A similar dropoff in reflection occurred 11–16° on each side of vertical. The result was the same when 2 cc of Freon were removed. Our interpretation is that there is

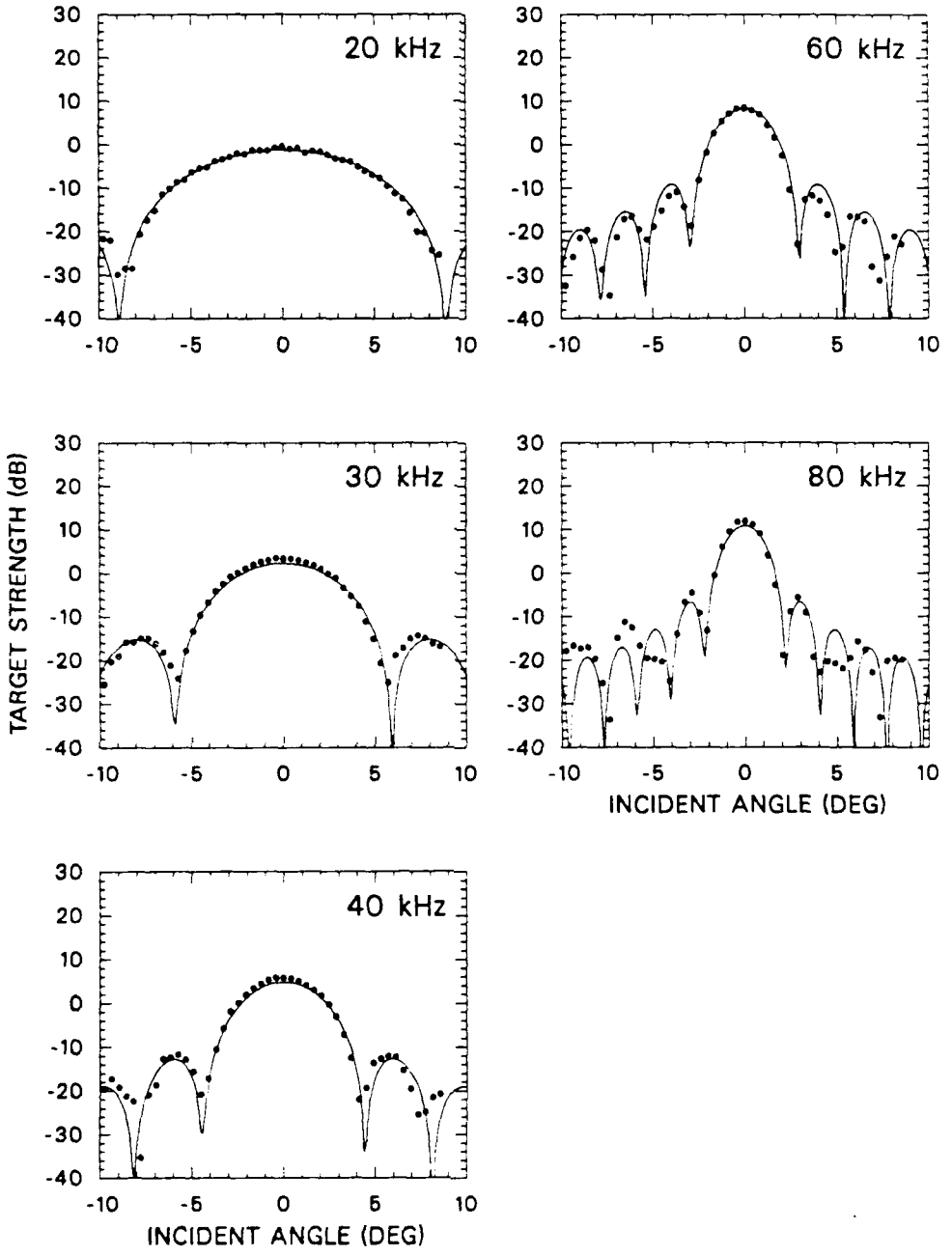

Figure 13. Air block returns from a 28-cm diameter area, Line N13. Solid line is theoretical pattern.

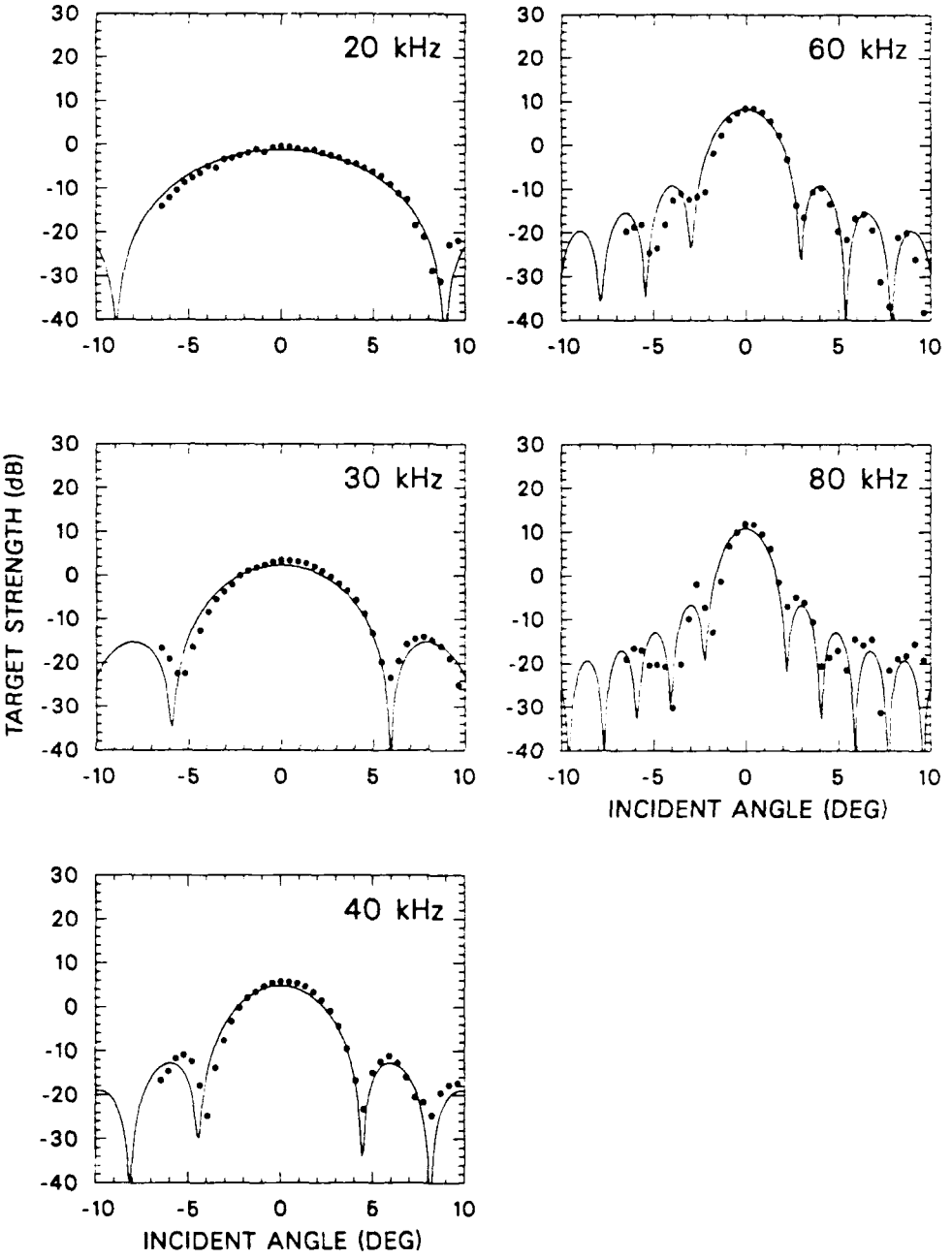

Figure 14. Air block returns from a 28-cm diameter area, Line E34. Solid line is theoretical pattern.

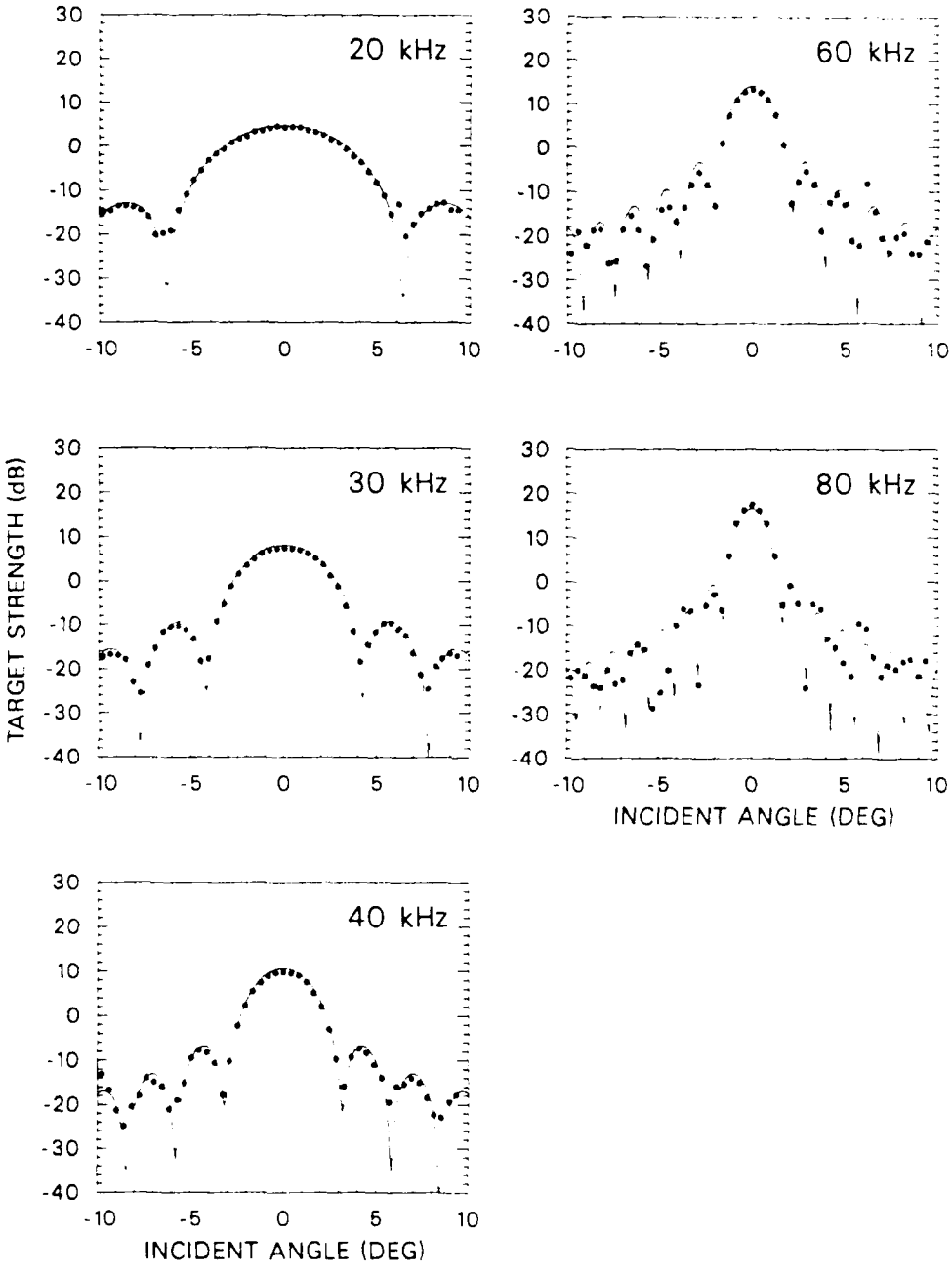

Figure 15. Air block returns from a 40-cm diameter area, Line N13. Solid line is theoretical pattern.

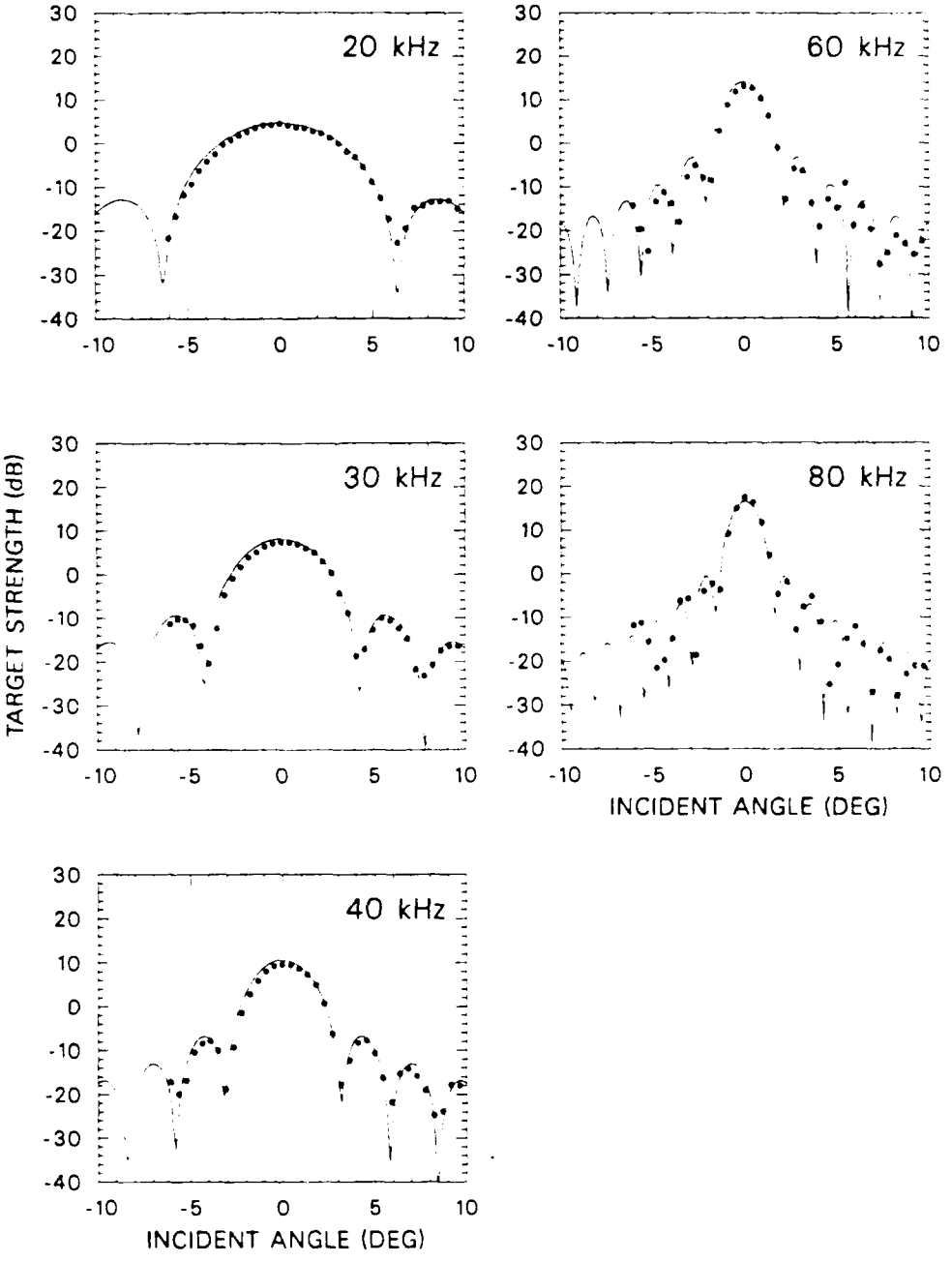

Figure 16. Air block returns from a 40-cm diameter area, Line E34. Solid line is theoretical pattern.

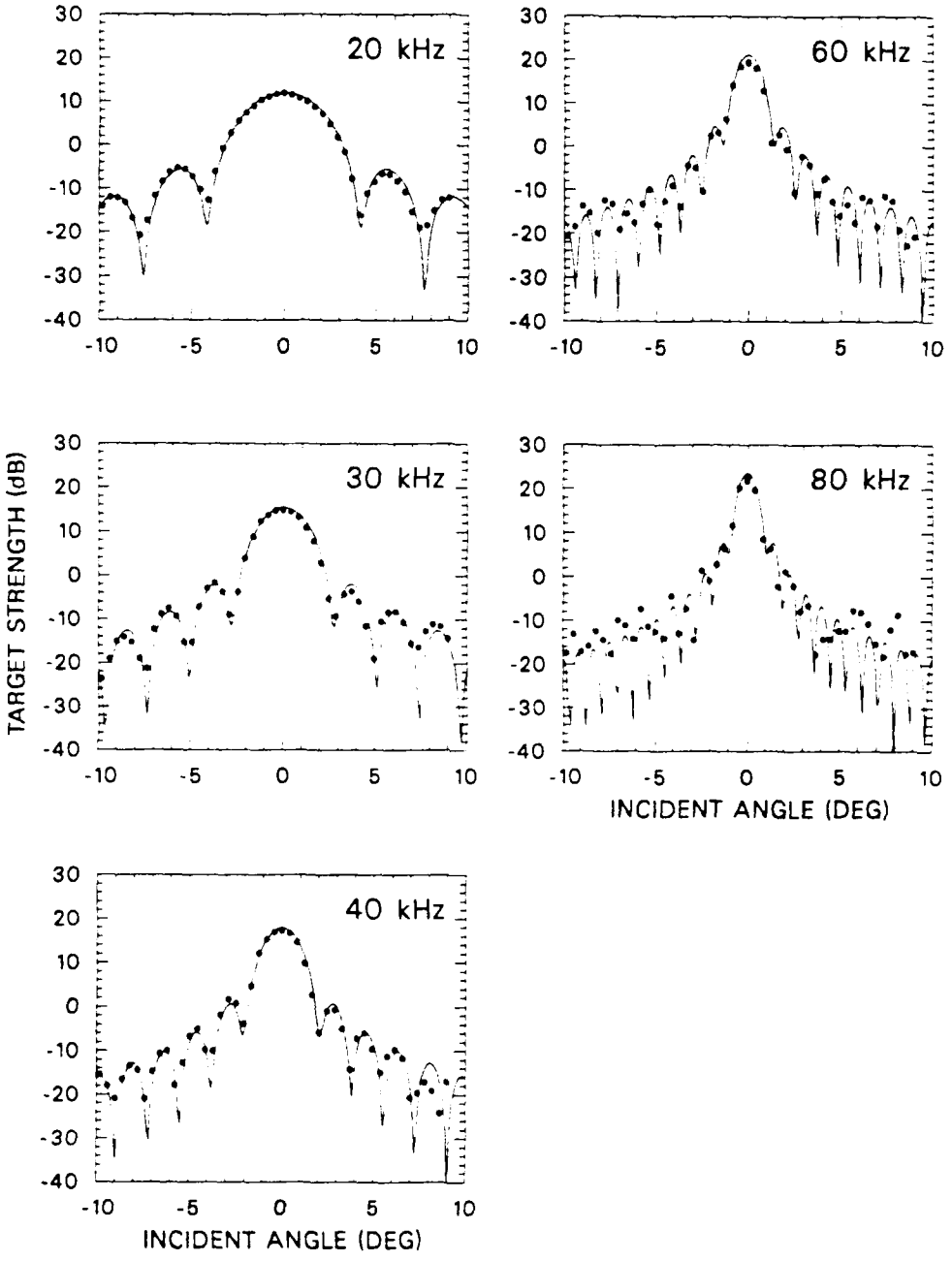

Figure 17. Air block returns from a 60-cm diameter area, Line N12. Solid line is theoretical pattern.

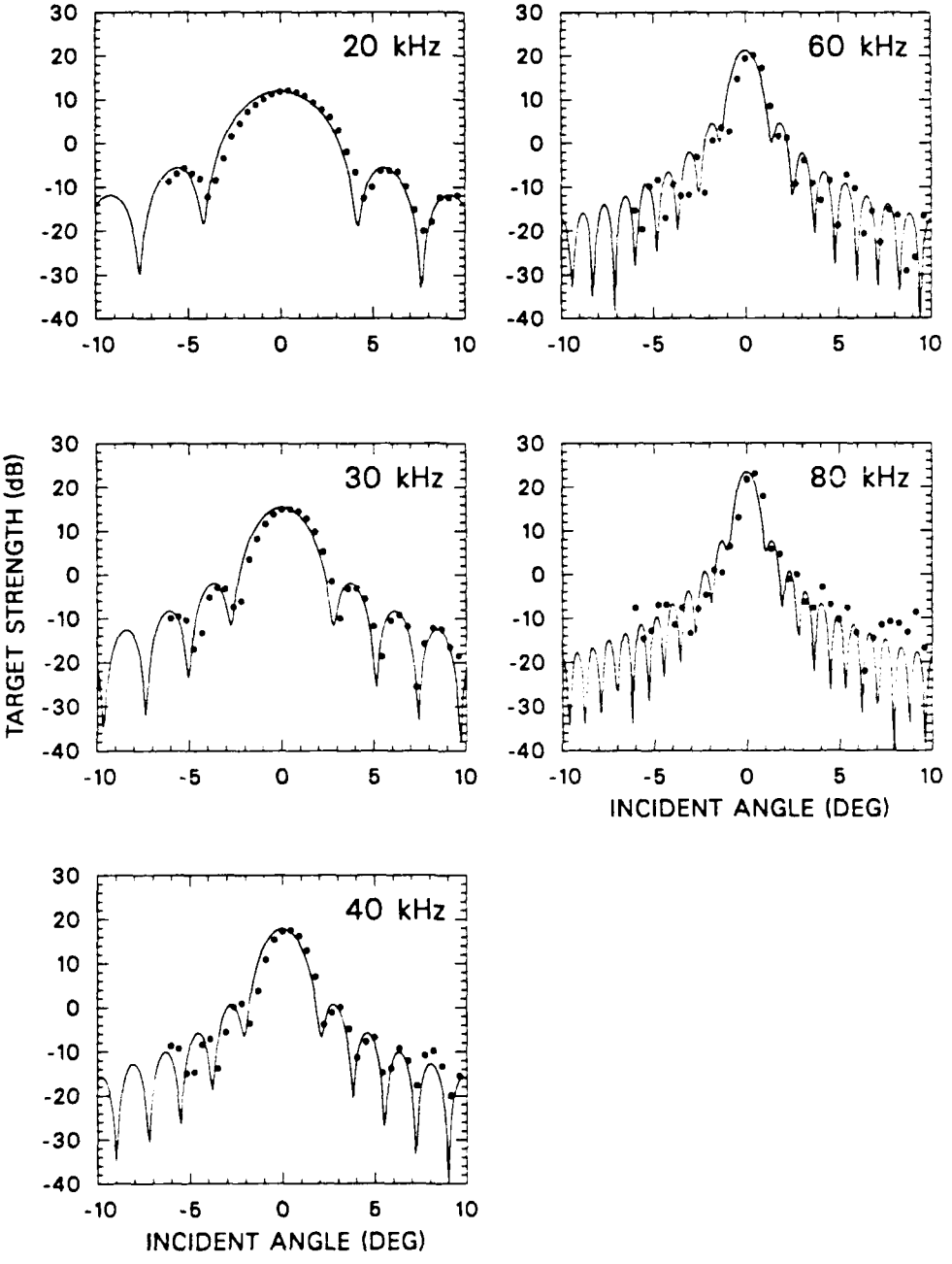

Figure 18. Air block returns from a 60-cm diameter area, Line E34. Solid line is theoretical pattern.

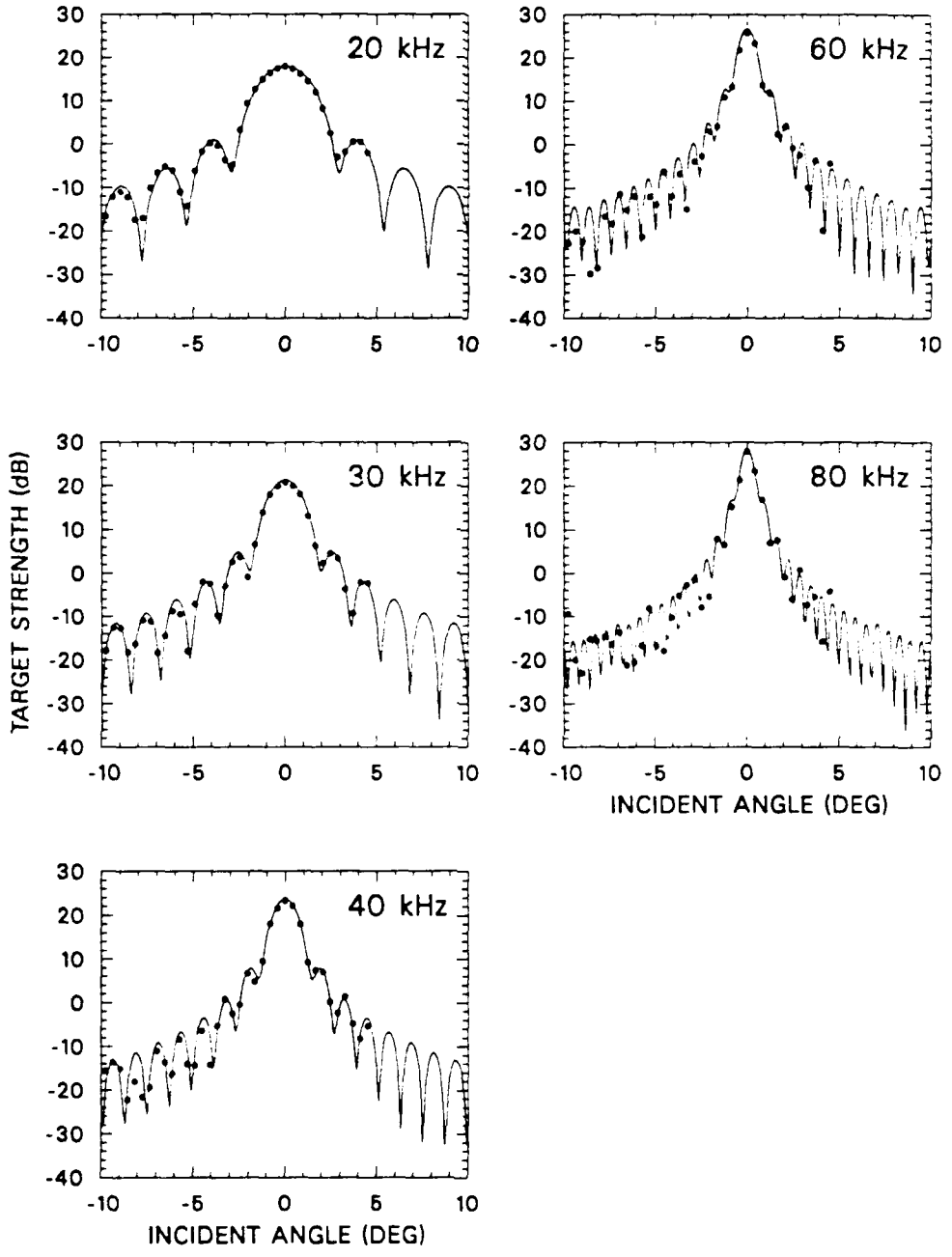

Figure 19. Air block returns from an 86-cm diameter area, Line N13. Solid line is theoretical pattern.

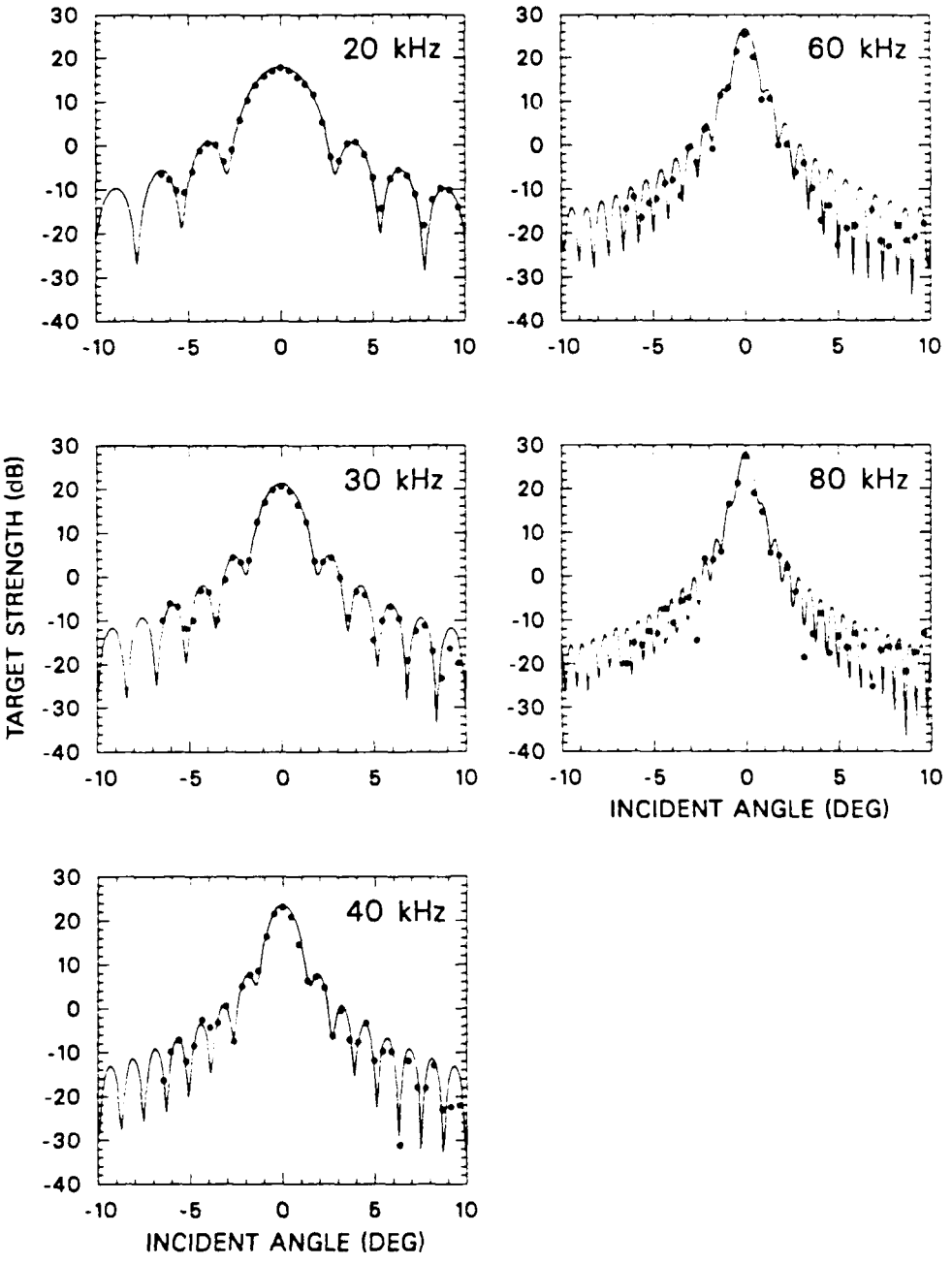

Figure 20. Air block returns from an 86-cm diameter area, Line E34. Solid line is theoretical pattern.

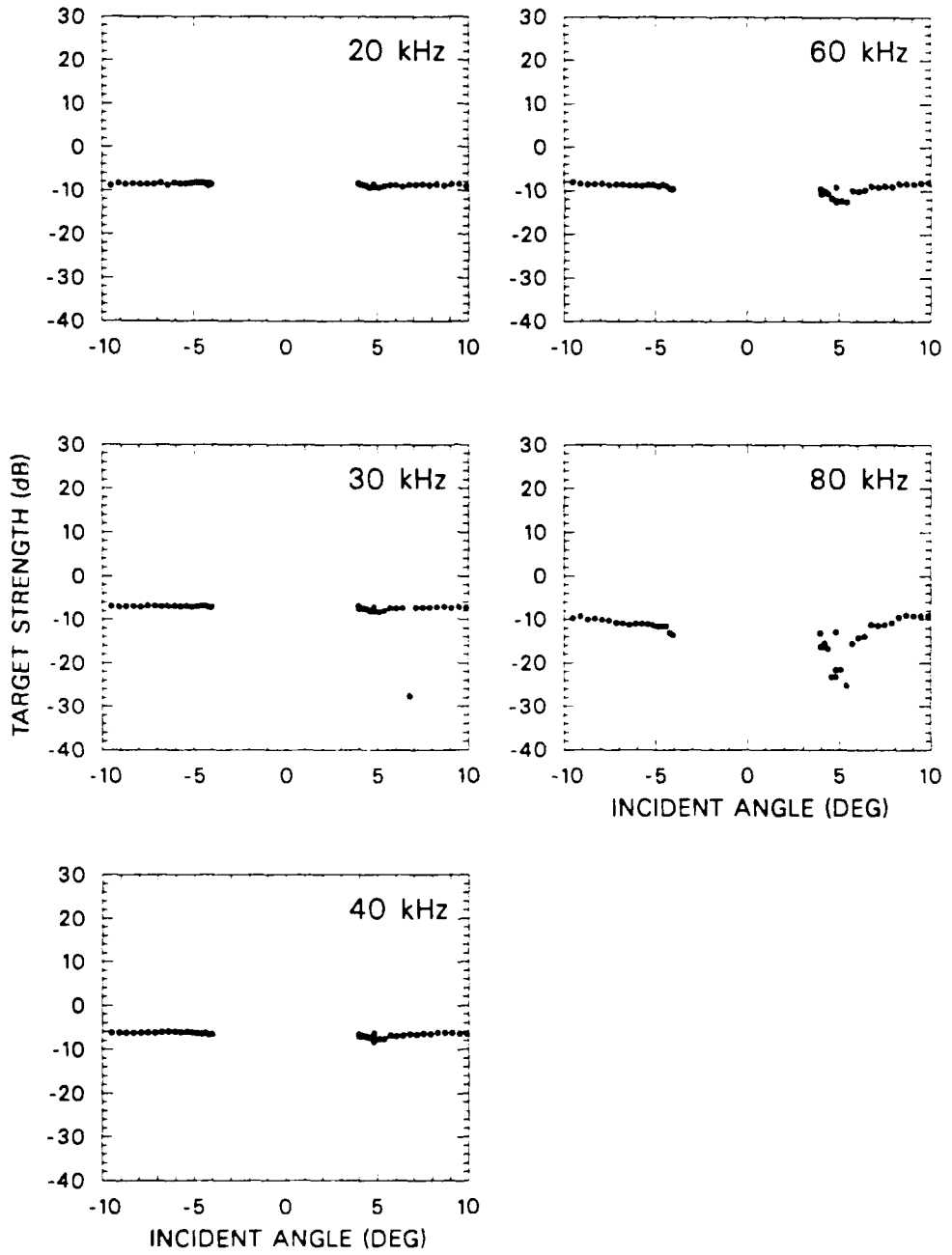

Figure 21. The measured target strength of the sphere during a pass of the transducer beneath an ice block. Because the sphere was spaced a few meters from the ice block, the incident angle was never zero, which corresponds to a vertical transmission. Thus the dots on each side of the gap were actually adjacent measurements. Run 10, Line N13.

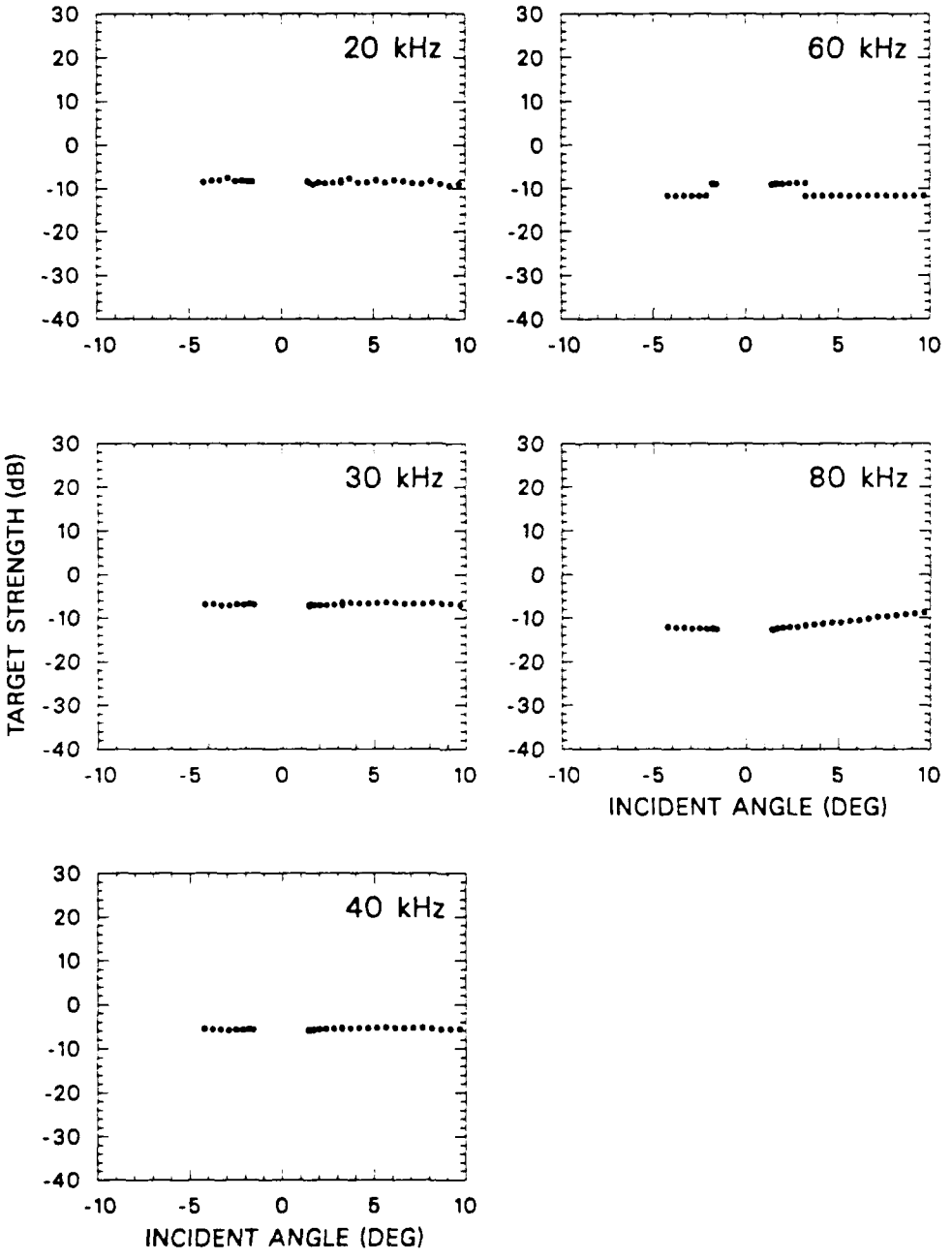

Figure 22. The measured target strength of the sphere when it was nearly overhead during a pass of the transducer beneath an ice block. Run 2, Line E22.

an actual dropoff in reflectivity at about 11° off the axis passing through the sphere's connector, and that this angle was obtained in the field as a result of the sphere being not only off to one side but also tilted by the current.

The average target strengths of the sphere reflections are plotted in Figure 23 for one of the two perpendicular lines of every run. At 80 kHz, the anomaly was often so extensive that a good reading could not be obtained. The true reading was probably 1–2 dB higher than shown but not high enough to continue the trend in the 20, 30, and 40 kHz readings. Measurements in Lake Union at the APL acoustic calibration barge showed an average target strength of −10 dB with a spread of 4 dB over the 20–80 kHz frequency interval and a slight indication of the 20–40 kHz rise seen in Figure 23. The index of refraction between the water and the Freon in the sphere changes significantly with temperature such that a better focus is obtained at arctic temperatures. This accounts for the higher target strengths of the sphere in the Arctic, where the temperature was near −2°C compared with 12°C for the lake tests.

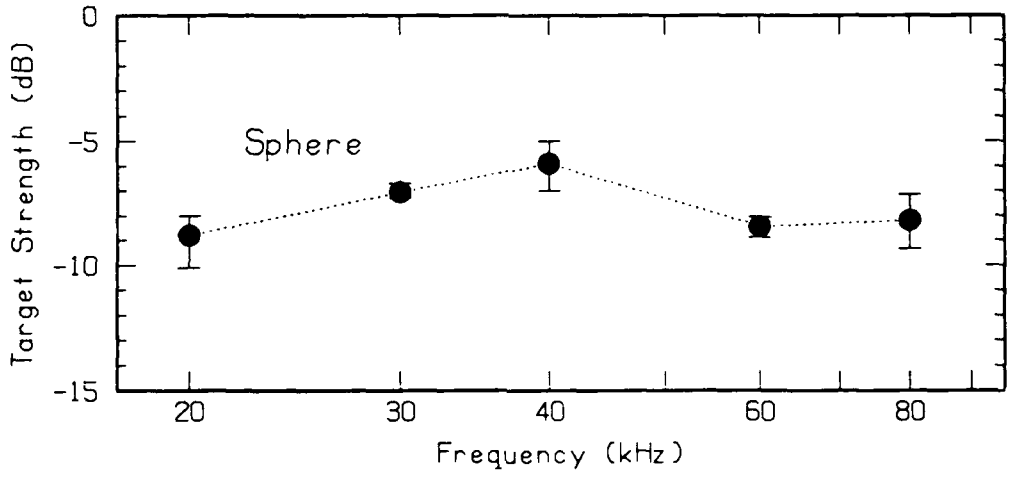

Figure 23. Average target strength of the calibration sphere at several frequencies, as measured in the field. The spread in readings is indicated by the bar.

V. MEASUREMENTS

Each run consisted of moving the transducer along two perpendicular lines by passing the ring both ways through the peg position that gave the highest return from the block. At each peg position, five frequencies were transmitted at a spacing of 0.1 s. The return was recorded on a Nicolet oscilloscope which digitized the envelope of the return signal at a 100-kHz rate. The digital record was then stored on a diskette for later processing. During processing, the return was examined and the average amplitude over the length of the pulse was determined. The target strength of the block was then calculated for each ping from the geometry, the transducer calibration, the transmit voltage, and the gain of the system. For each peg position, the location of the transducer with respect to the block was calculated and used to compute the vertical angle of incidence. Plots were then made of target strength versus that angle. The reflections at normal incidence are discussed in the next section.

All the plots for the natural ice blocks (Runs 1, 2, 3, and 5) are shown in Figures 24–31. The solid lines are the theoretical return for a perfectly flat circular plate with the same diameter as the block (but computed numerically). There is always a central peak and some indication of side lobes at all frequencies. There are two points near zero incidence because we started each run at zero and moved in one direction, then repeated a measurement at zero as we started moving in the opposite direction. The slight discrepancy is due to experimental error.

Runs 4–8 and 14 involved special preparation of the blocks as described in the following paragraphs. Run 4 was a repeat of Run 3 after the 84-cm block had been in place overnight. During Run 3, we noticed an extra reflection that sometimes interfered with the ice block reflection. The next morning we determined that the interference was caused by a cable used in an experiment in the adjoining area. This cable was raised to move it out of range, and the measurements were redone. Run 4 gave much lower returns (Figures 32 and 33). The Run 3 data were later examined to remove any readings which might have been altered by the cable echo. The difference between the Run 3 and Run 4 results is apparently due to some change that occurred in the skeletal layer during immersion overnight. The changes with time are discussed in Section VI.B.

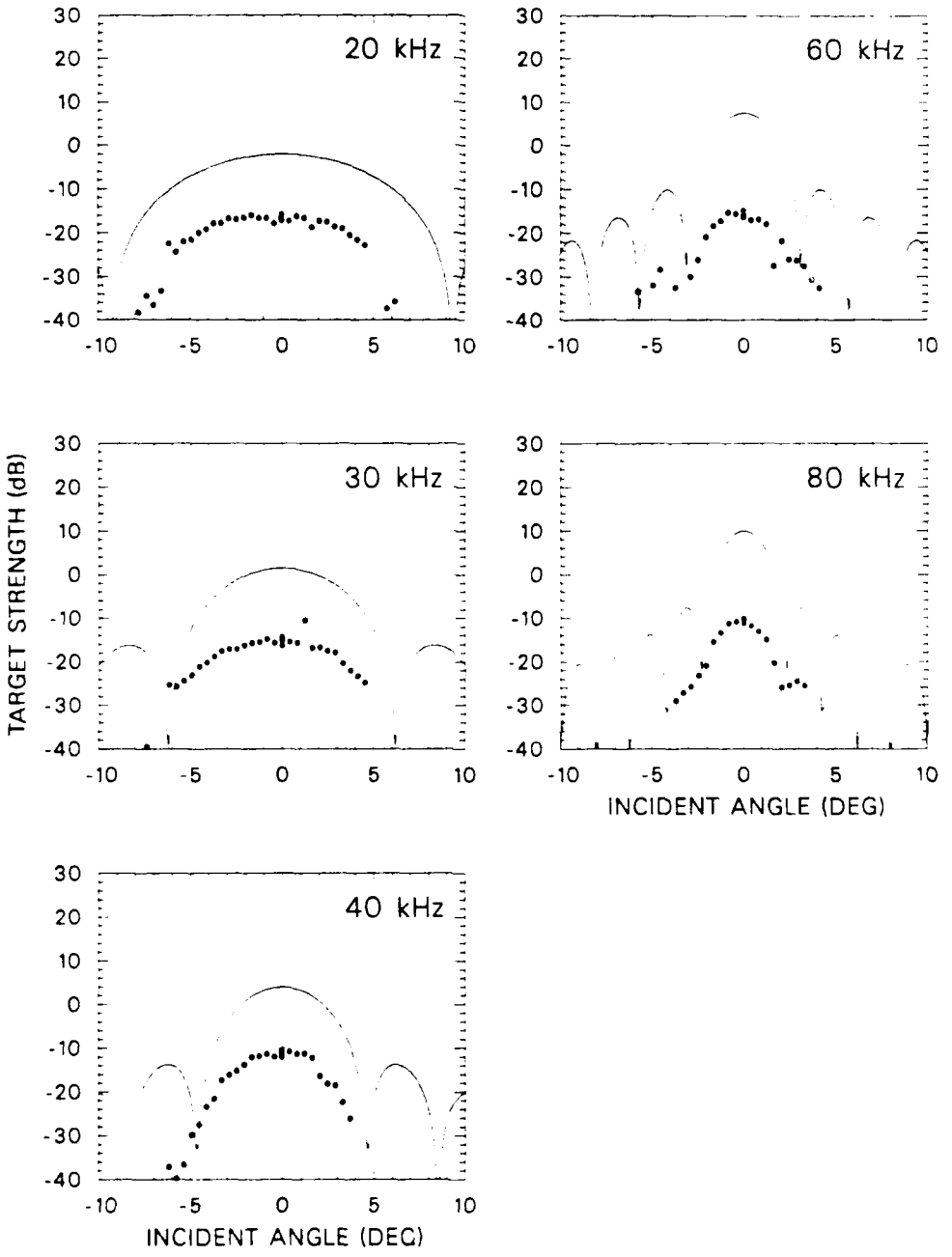

Figure 24. Target strength measurements of the 27-cm ice block. Run 2, Line N12.

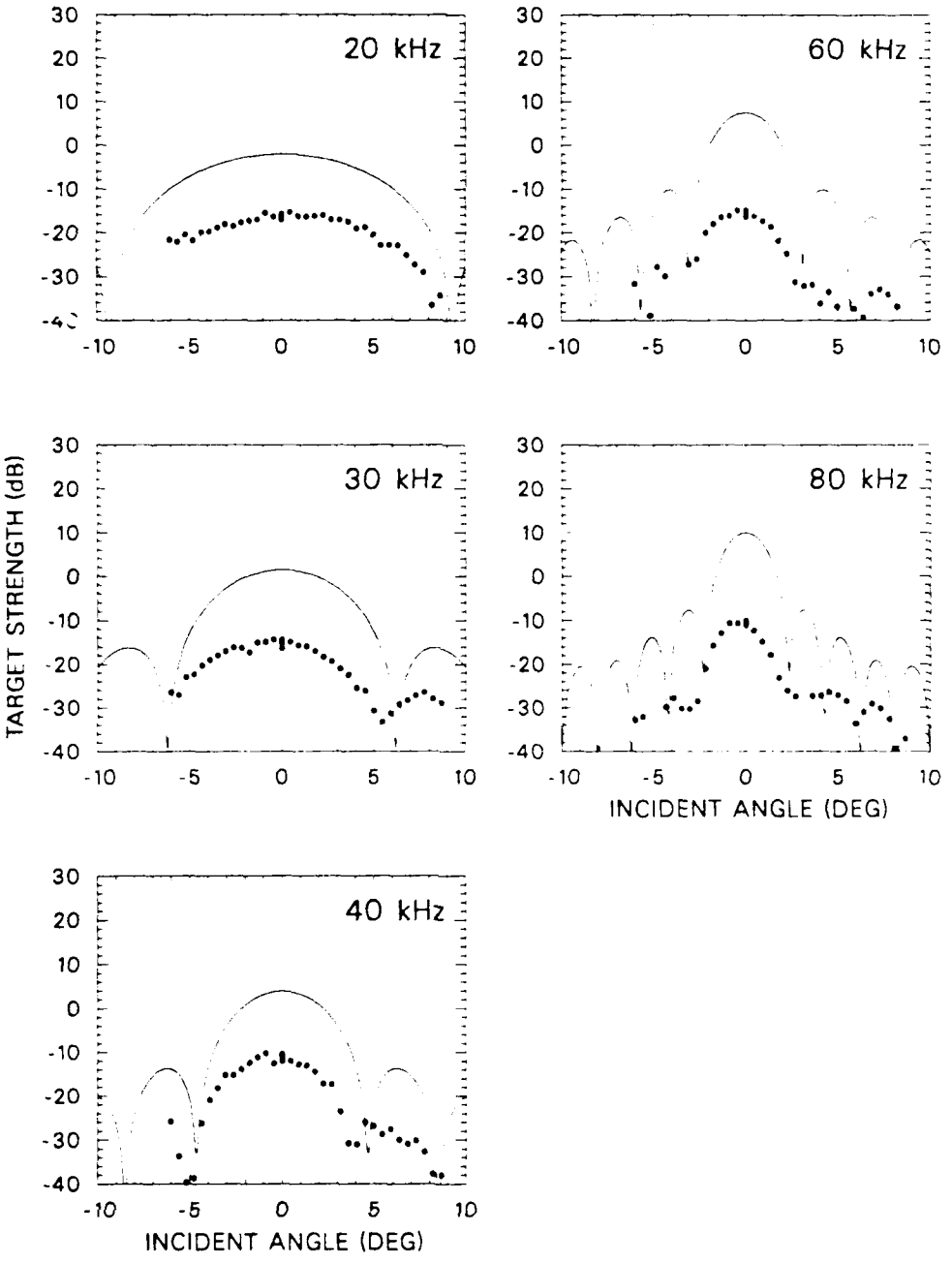

Figure 25. Target strength measurements of the 27-cm ice block. Run 2, Line E22.

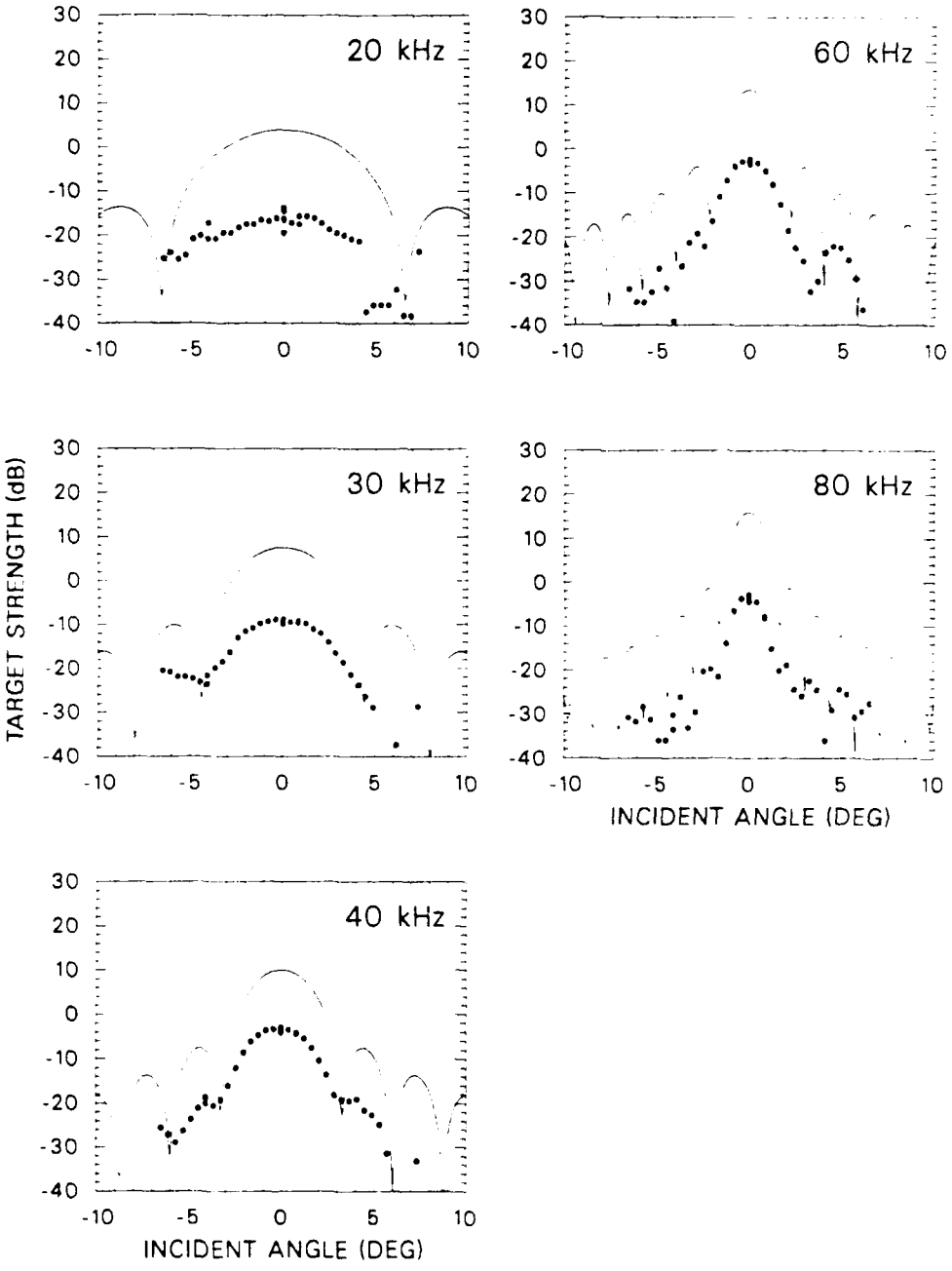

Figure 26. Target strength measurements of the 38-cm ice block. Run 1, Line N14.

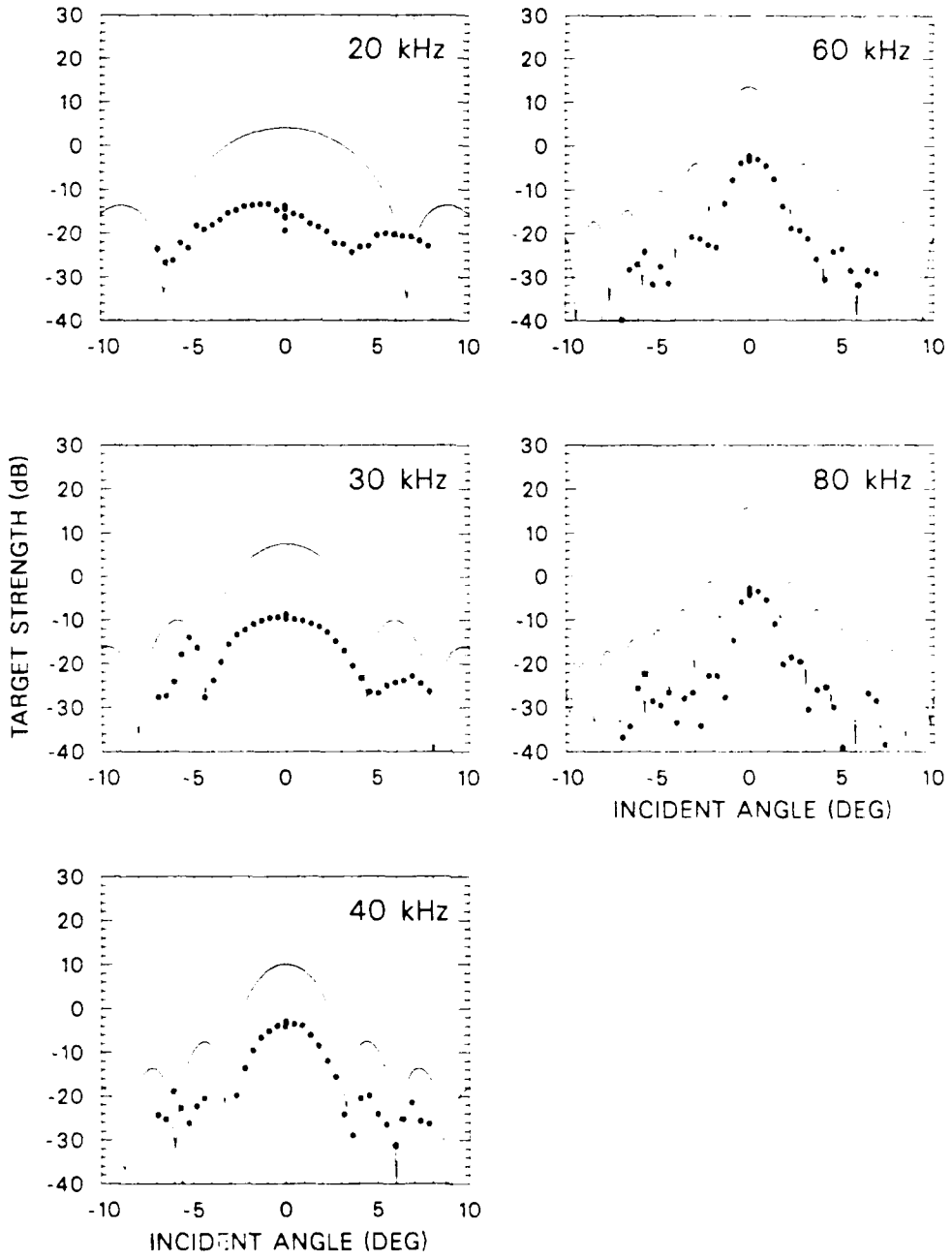

Figure 27. Target strength measurements of the 38-cm ice block. Run 1, Line E17.

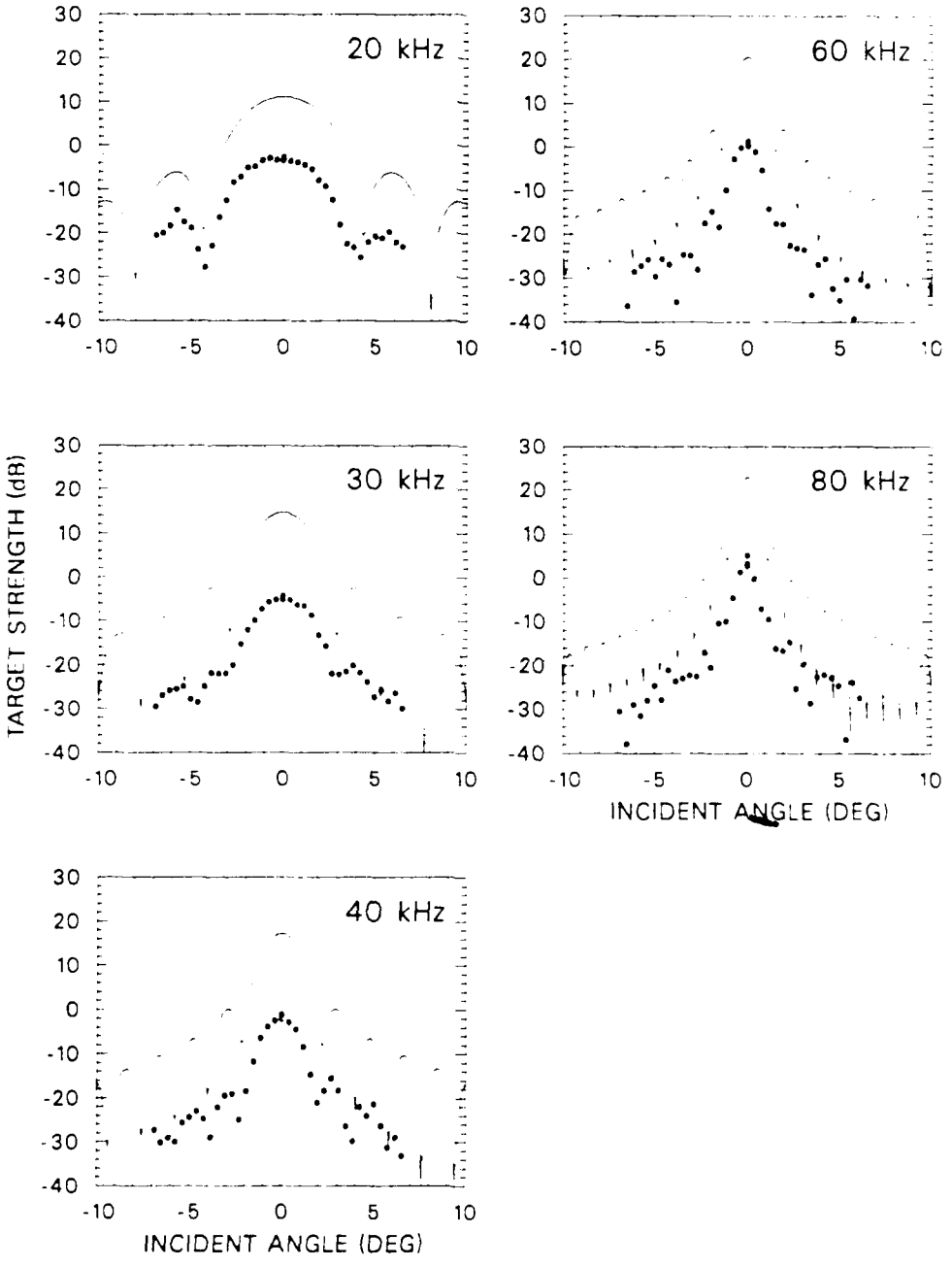

Figure 28. Target strength measurements of the 58-cm ice block. Run 5, Line N27.

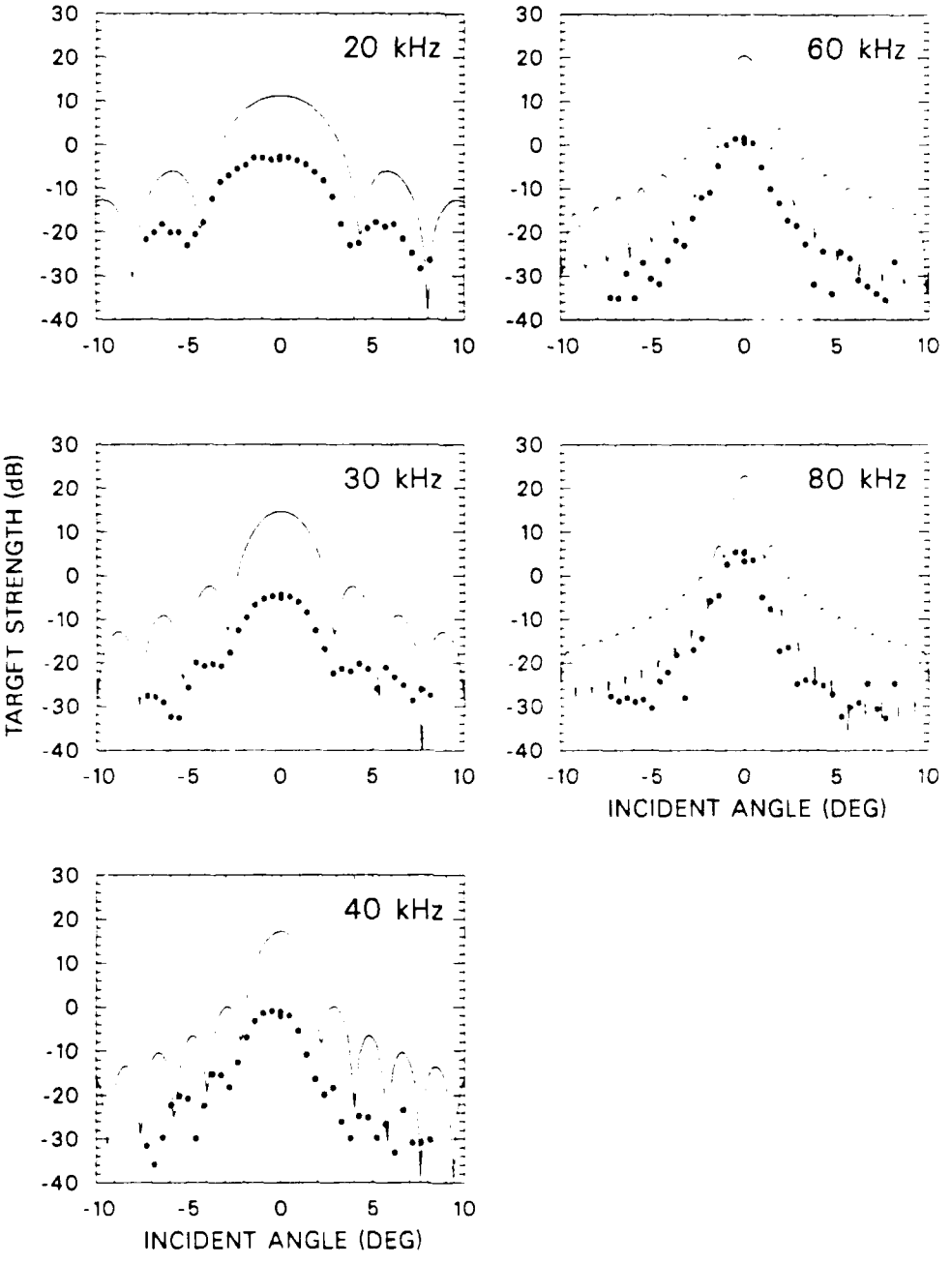

Figure 29. Target strength measurements of the 58-cm ice block. Run 5, Line E31.

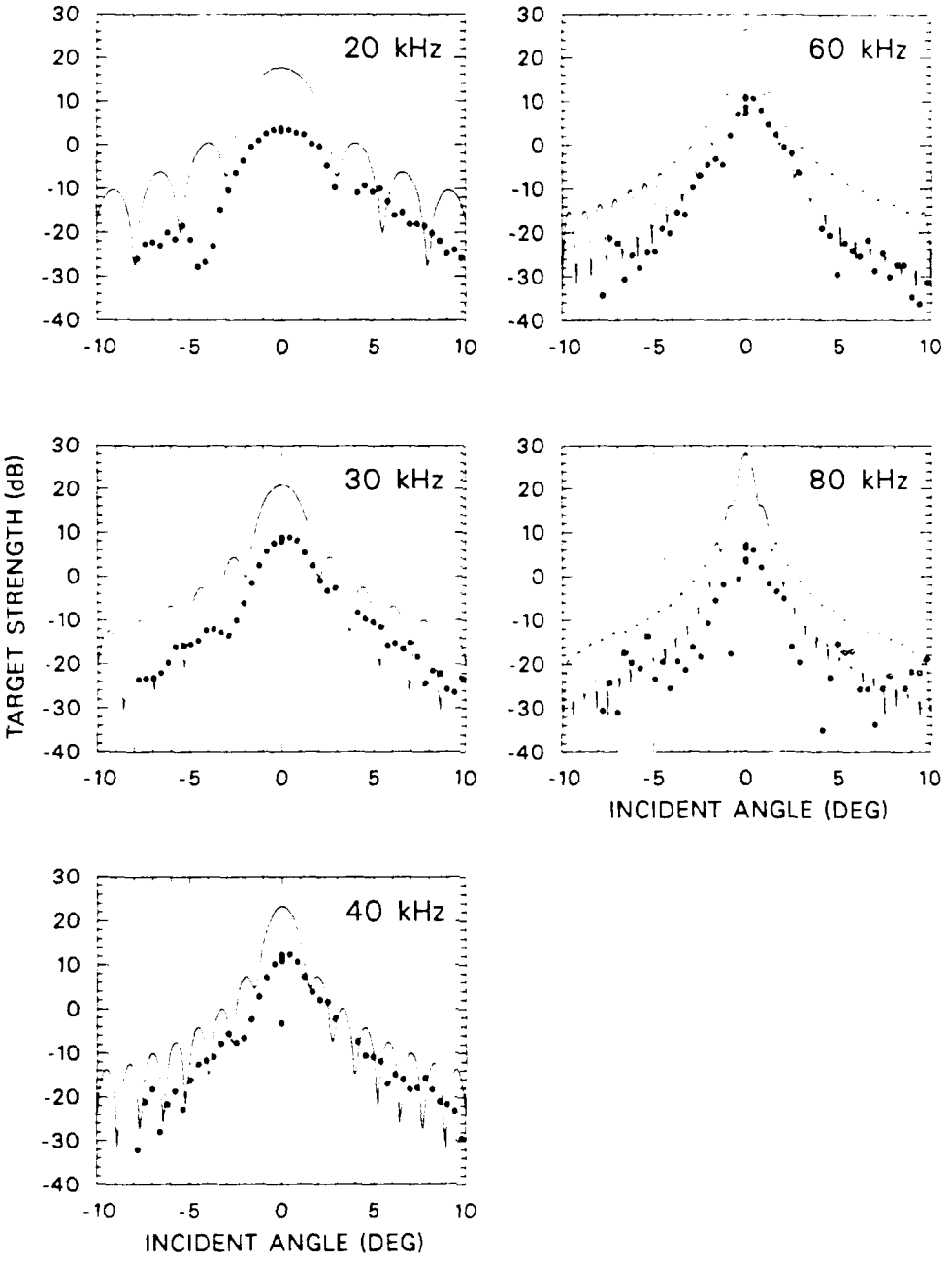

Figure 30. Target strength measurements of the 84-cm ice block. Run 3, Line N12.

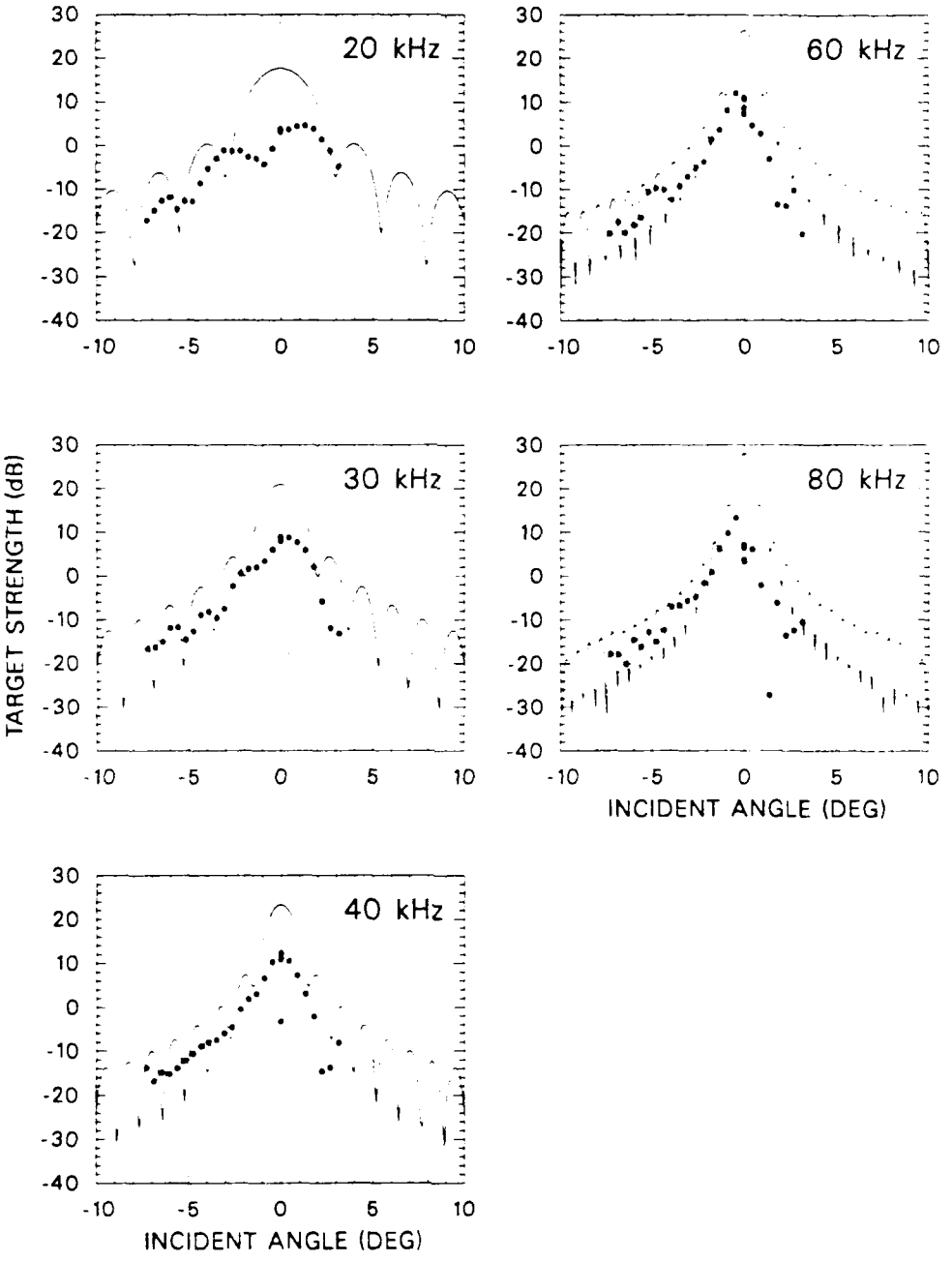

Figure 31. Target strength measurements of the 84-cm ice block. Run 3, Line E33.

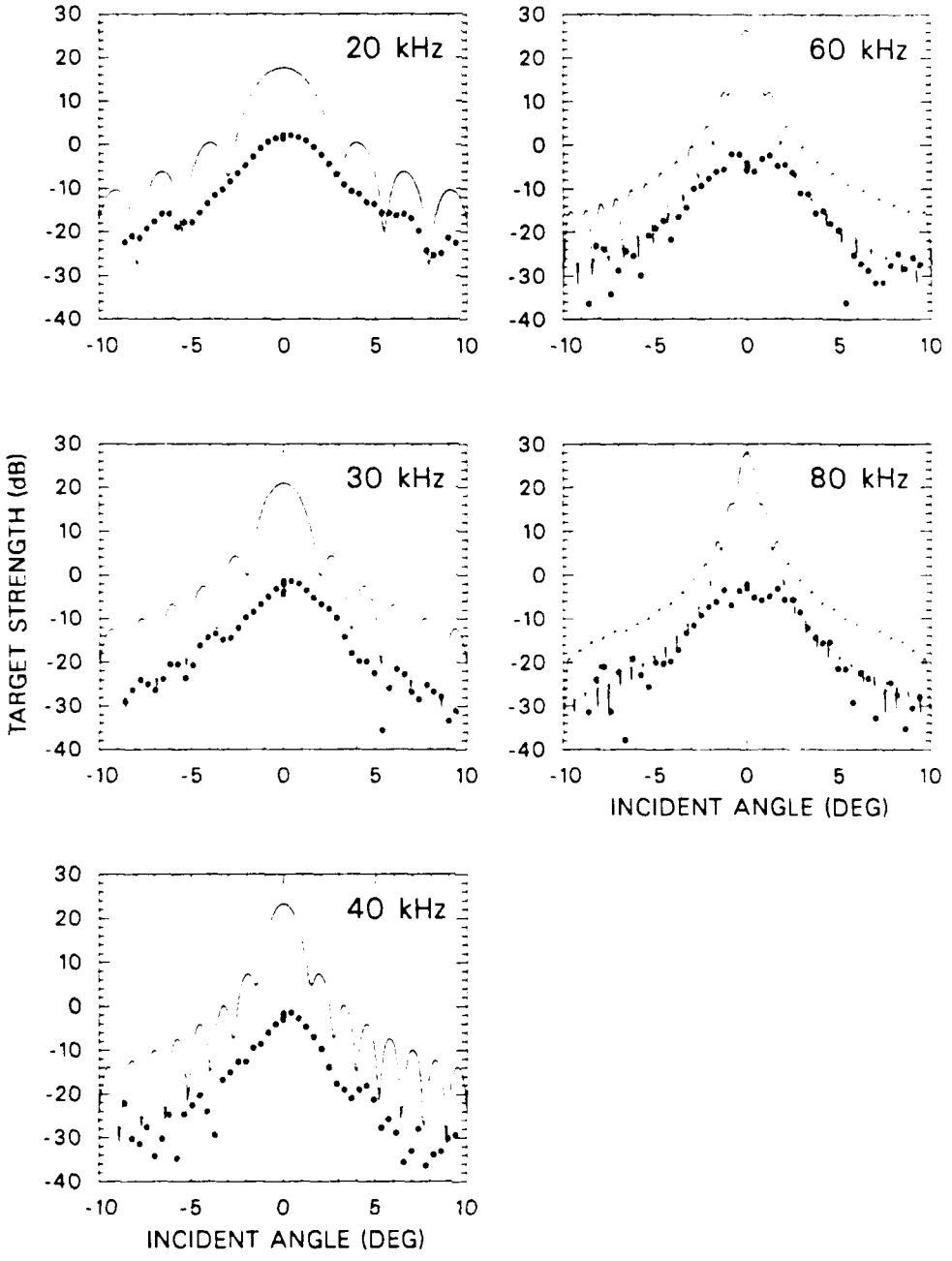

Figure 32. Target strength measurements of the 84-cm ice block after it had remained in place overnight. Run 4, Line N12.

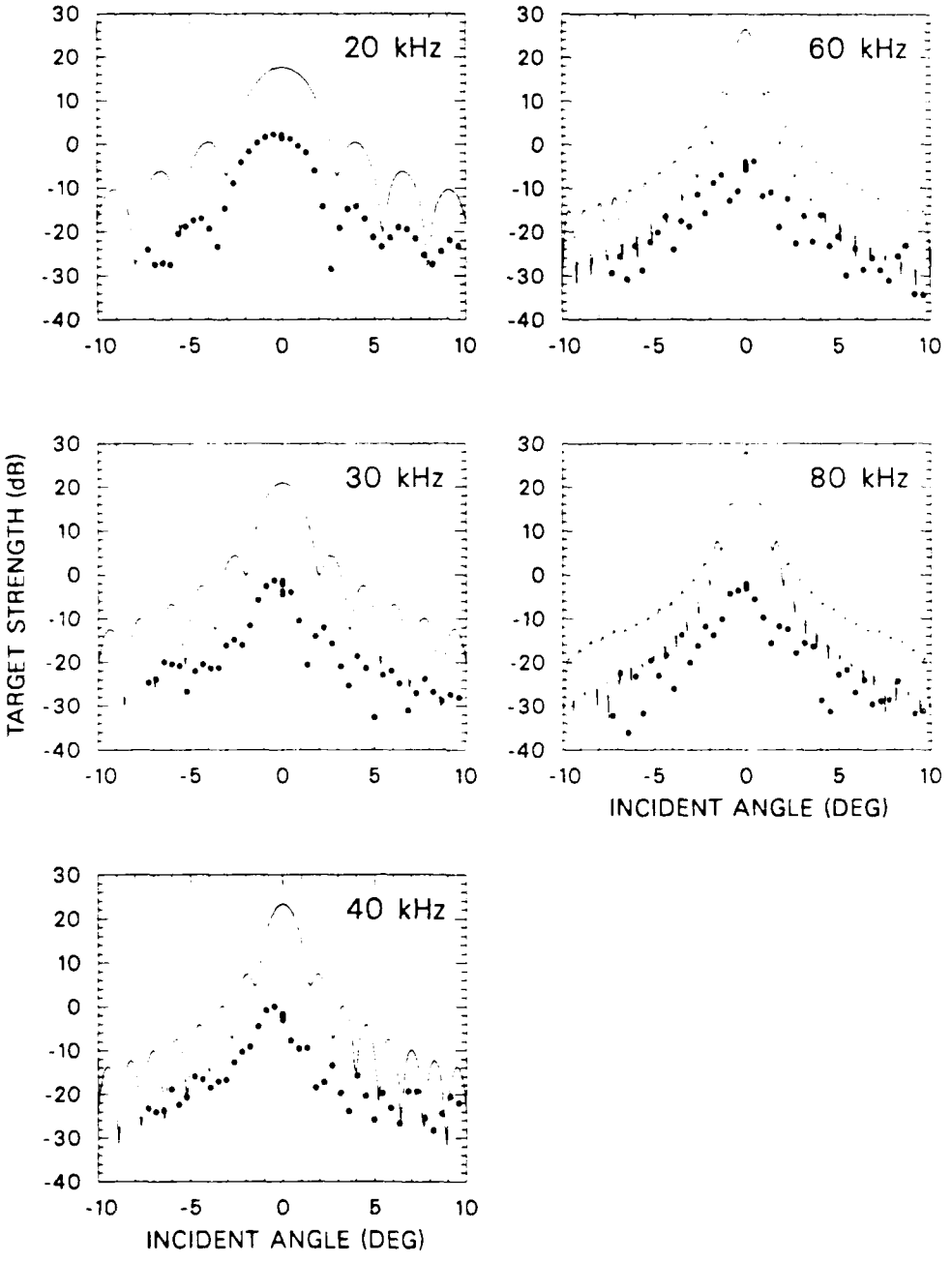

Figure 33. Target strength measurements of the 84-cm ice block after it had remained in place overnight. Run 4, Line E33.

Prior to Run 4, an underwater TV camera was installed to view the ice block. The bottom of the block was examined from several angles and appeared to be flat. When the block was removed and examined closely, the bottom also appeared to be flat. Measurements a few hours later (described in Section VIII.B) showed it to be a plane surface with deviations of only 2–3 mm.

Following Run 5 with the 58-cm block, we left the block in place and monitored returns over the next 15 hours to see if we would observe the same decrease seen for the larger block. As discussed in Section VI.B, the results did decrease with time, although not as much as for the 84-cm run.

The purpose of Run 6 was to determine what effect air trapped in the skeletal layer had on the reflectivity of the surface. After Run 5, the 58-cm block was raised until nearly out of the water, and insulation was packed around the block and between it and the edge of the hole to prevent air from circulating below the block. This insulation was kept in place as the block was raised just out of the water. The block was allowed to drain for 40 minutes, relowered, and positioned for measurement. The results (Figure 34) show a considerable increase in reflectivity but a poorer pattern. The returns at normal incidence are discussed in Section VI.C.

The purpose of Run 7 was to determine if a block could be removed and reinstalled without changing the reflective properties of the skeletal layer. A lifting band was fastened around the block used in Run 6 so it could be removed and positioned horizontally for sawing. A frame (Figure 35) was constructed to provide a flat cut with a chain saw; however, we were unable to control the flexing of the 5-ft saw blade, resulting in a slightly curved and somewhat rough surface. While the block was in the air, a band of fiberglass insulation was placed around the lower end and a circular plug of insulation fit over the bottom. The block was hoisted out and moved to a platform about 10 m away, where the top portion was cut off with a chain saw to reduce the block to a manageable size. The block was moved to the 84-cm hole and lowered upside down into the water as the insulation was removed. Our intention was to push the block below the ice, let it remain inverted for a while to allow the air to escape, and then turn it over. The question was whetner the skeletal layer would retain its original reflective properties during this procedure.

After the block was pushed below the ice, the current swept it sideways, but we were able to pull it back up into the hole. We raised it nearly out of the water, keeping

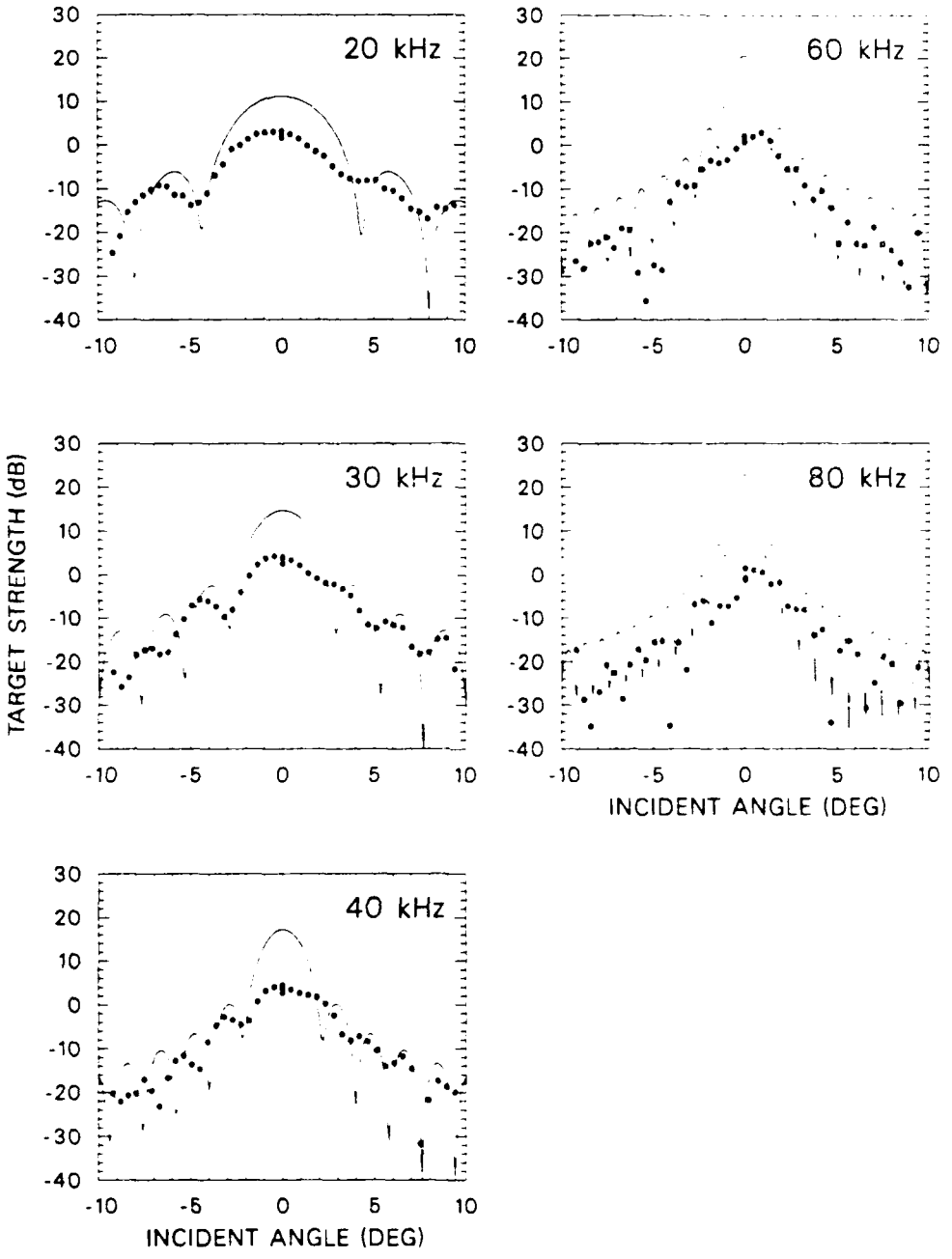

Figure 34. Target strength measurements of the 58-cm ice block after it had been drained and relowered. Run 6, Line E32.

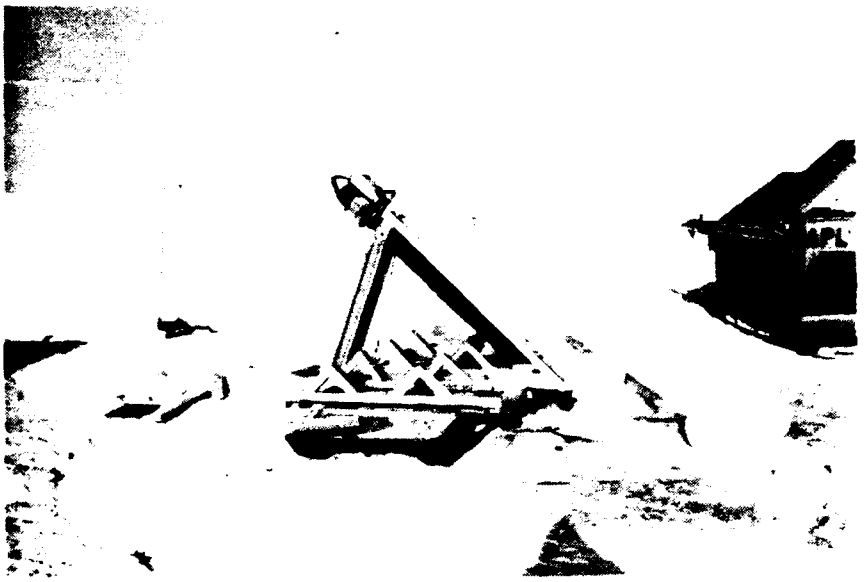

Figure 35. Chain saw and frame used to cut off portions of the ice blocks.

the skeletal layer submerged, and repositioned the lifting band. On the next try, the block was successfully turned over. We raised it part way out of the water again and removed the lifting band. The air pan was then placed over the floating block, and the pole attached to the pan was used to force the block down again. When in place, air was added to the pan to provide an air chamber above the block and increase the reflection from the back face. Reflections were measured in the usual manner and found to be very high with a good pattern (Figure 36).

For Run 8 we removed the block from the hole and cut off the skeletal layer and transition zone. The block was pushed down again with the pan which was then filled with air. The measurements showed very low reflection at all frequencies (Figure 37). The patterns indicate that the transducer path did not go through the axis of the block face, invalidating the results.

The final measurement, Run 14, was made using a 58-cm block that had been removed 4 days earlier and left on the surface to cool. It was sawed off square on both ends, giving a length of 62 cm, and pushed down with the pan, which was then filled with air. The reflections (Figure 38) were as strong as for Run 7 except for a dropoff at 80 kHz. (A comparison of normal-incidence returns is given in Section VI.C.)

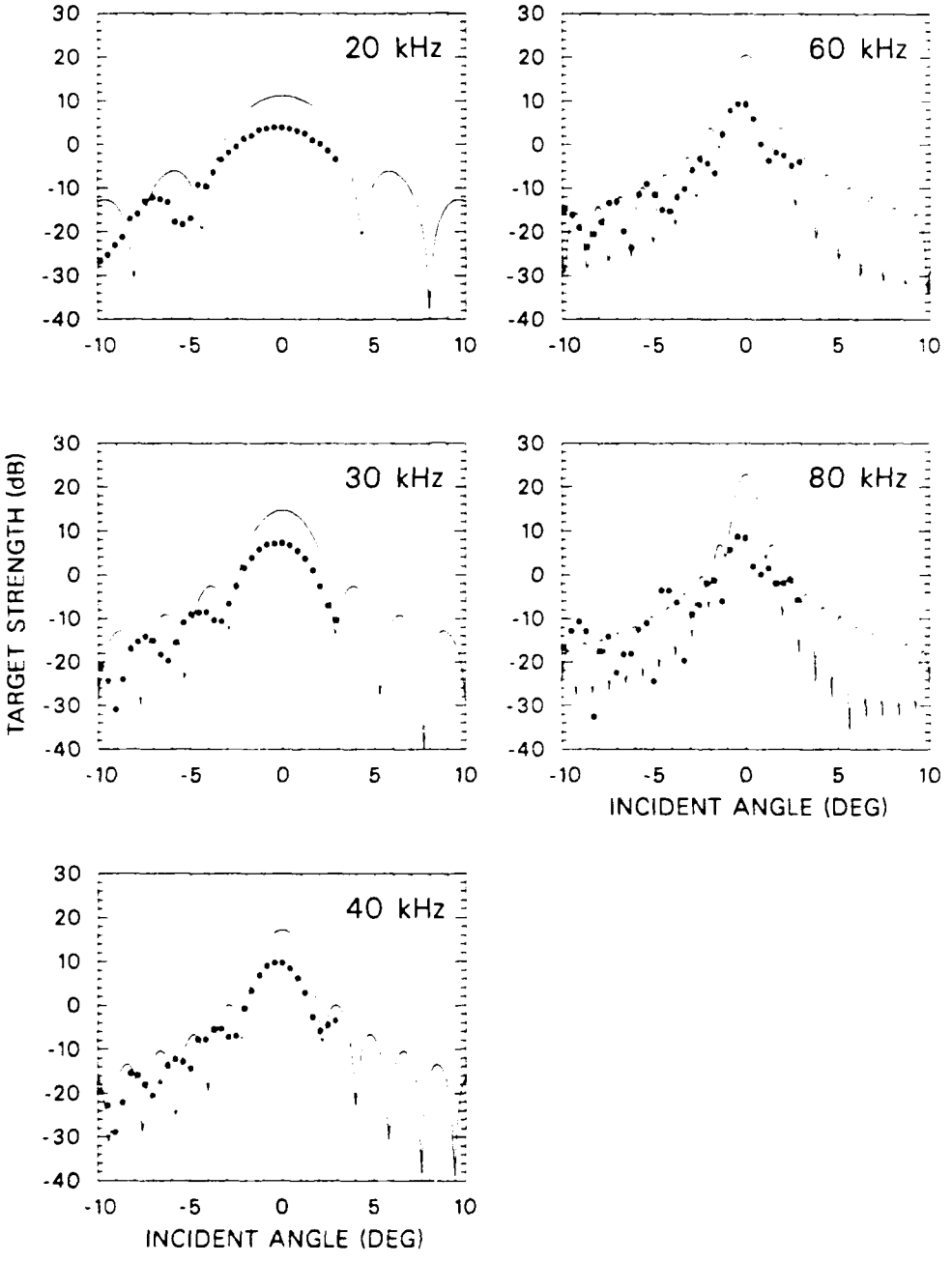

Figure 36. Target strength measurements of the 58-cm ice block after sawing off the upper end, lowering the block upside down to release trapped air, and turning it right side up under water. Run 7, Line N11.

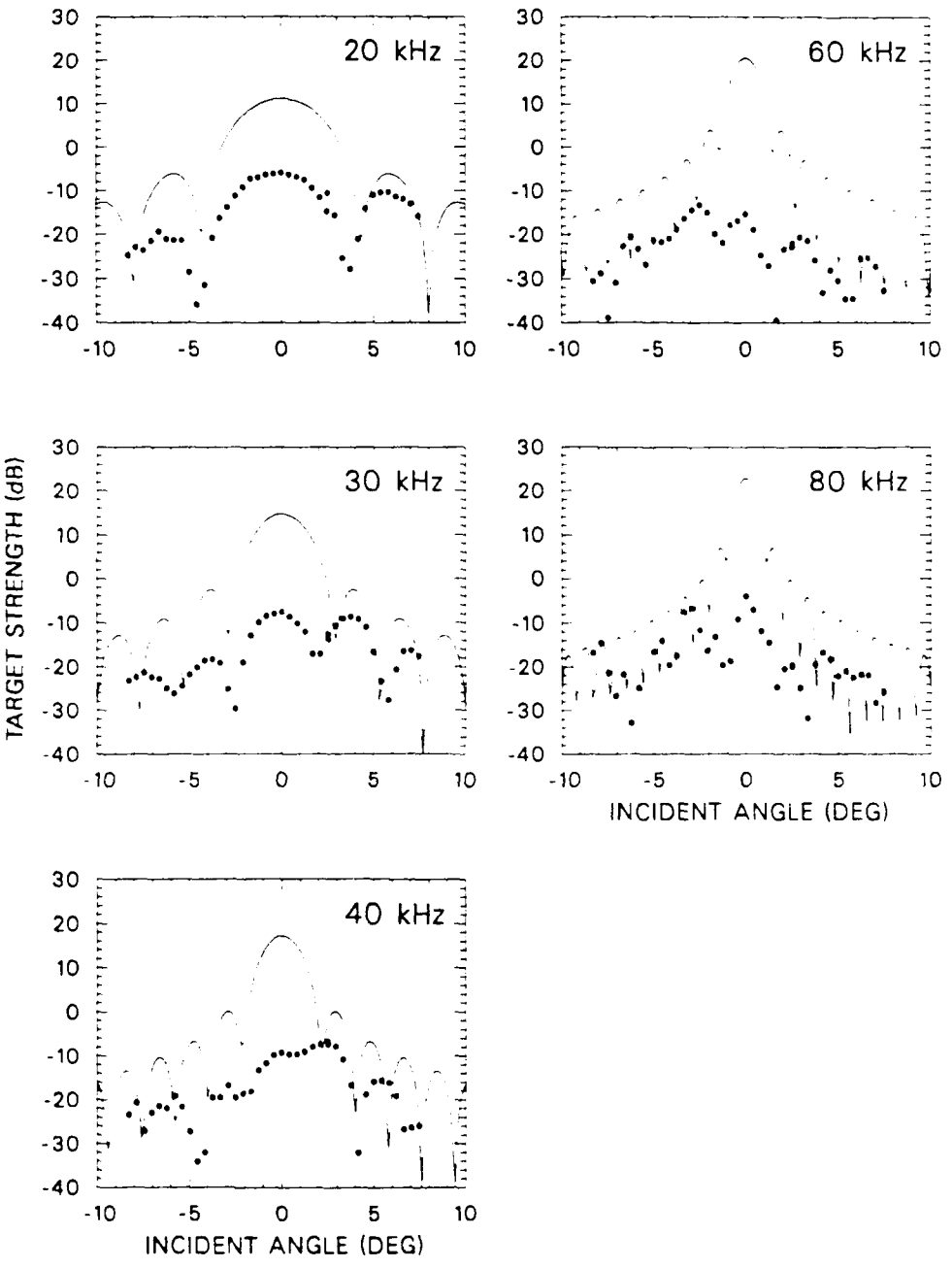

Figure 37. Target strength measurements of the 58-cm ice block with the skeletal layer sawed off. Run 8, Line N10. Apparently the transducer did not pass through the axis of the block or else the saw cut gave a curved surface.

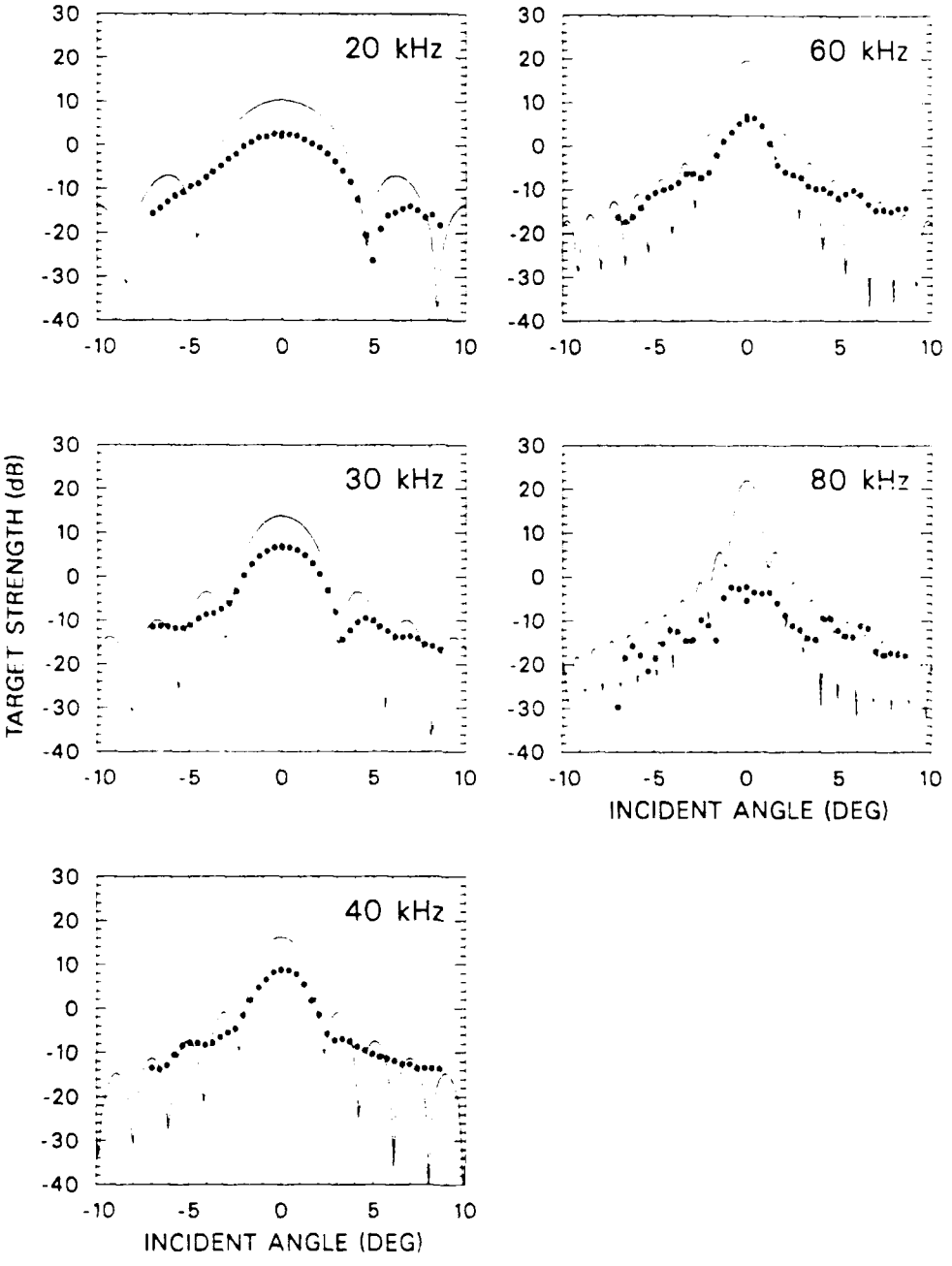

Figure 38. Target strength measurements of a 58-cm block formed by cutting off the ends of a block that had been in the cold air for 4 days. Run 14, Line N12.

VI. LOWER FACE REFLECTIONS

A. Skeletal Layer

The angular response patterns of reflections from the skeletal layer do not closely follow predicted peaks and nulls in the side lobes. In general, the more the reflection at normal incidence falls below the theoretical level, the fewer the details present in the pattern.

The results of the measurements conducted at normal incidence in 1986 are summarized in Figure 39. After an area correction based on the rigid plate equation, the results for the different sized blocks do not agree. The large blocks seemed to have a very low reflection, perhaps because the surface was not flat. The smallest block, 40 cm, had a very high reflection, which we attributed to diver air that had collected in the skeletal layer.

The 1988 results are plotted similarly in Figure 40 for comparison. The area normalization brings the results reasonably close together. (The spread is about 6 dB.) The variations between blocks in 1986 may have been caused by some undulations observed on the undersurface by the divers. Similar undulations were noticed in 1988; after the experiment, they were measured by divers (see Section VIII.A) and found to be sinusoidal in cross section with an amplitude of 3.8 cm and a wavelength of 8.5 m. Such undulations would have more effect on the returns from the larger blocks.

The reduction in the target strength of the ice block face caused by the character of the surface is represented by $-20 \log R_a$, where R_a is the amplitude reflection coefficient of the lower face. The R_a's corresponding to the 1988 measurements are shown in Figure 41. The average R_a for the four blocks decreases from 0.20 at 20 kHz to 0.12 at 80 kHz.

Because of the difference in acoustic impedance, a water-ice interface should reduce the reflection by 8 dB compared with that predicted from rigid plate theory, assuming a sound speed of 3700 m/s in the ice. The skeletal layer probably has a lower sound speed than the solid ice, but the speed would be difficult to measure. It would take an effective sound speed of about 2300 m/s in the skeletal layer to provide an impedance mismatch that would give the amplitude reflection coefficients shown in Figure 41. Part of the reduction, however, may be due to the surface not being flat.

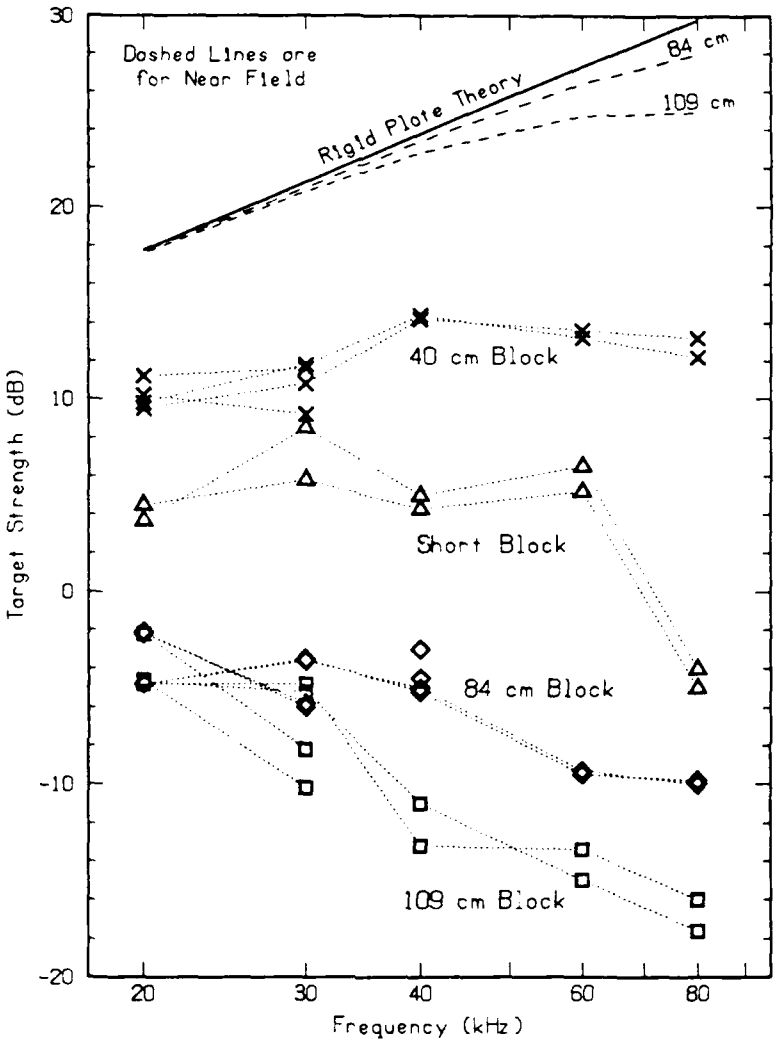

Figure 39. Target strengths at normal incidence for all blocks measured during an earlier experiment in 1986. A correction of 20log(area of 84-cm block / area of block face) has been applied to make the results comparable.

The 1988 reflections are higher than those measured in 1986. One observable difference between the 2 years was that in 1986 the transition zone of weak ice (when probed with a pointed tool) appeared to be about 15 cm thick compared with 10 cm in 1988. Also, the snow depth was more uniform over the refrozen lead used for the 1988 experiments, indicating the under-ice surface may have been flatter. Measured offsets of the block surface from a plane in 1988 had standard deviations of less than 1 mm for the 27 and 38 cm blocks and 2–3 mm for the larger blocks (see Section VIII.B).

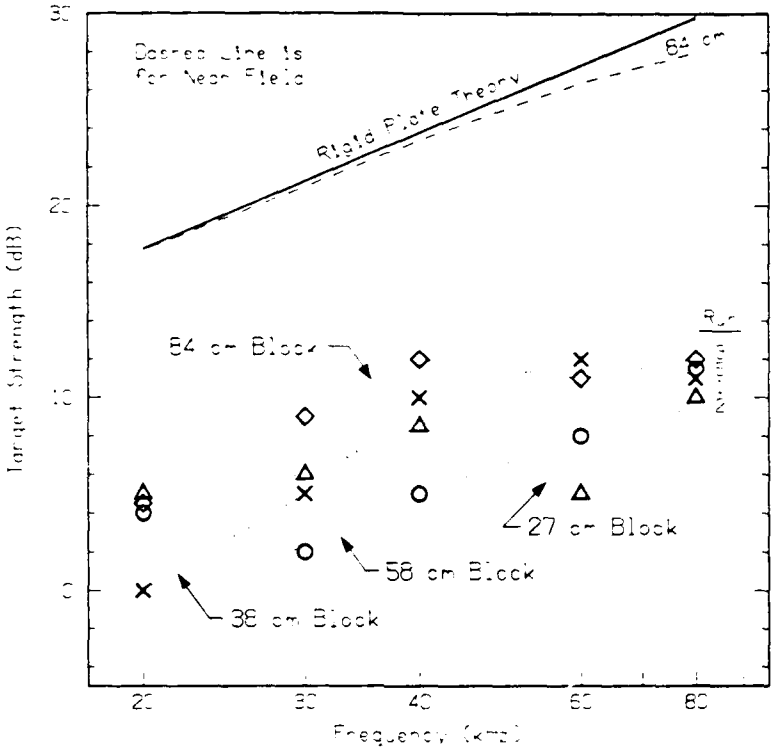

Figure 40. Target strengths at normal incidence for all blocks measured during the 1988 experiment. A correction of 20log(area of 84-cm block / area of block face) has been applied to make the results comparable.

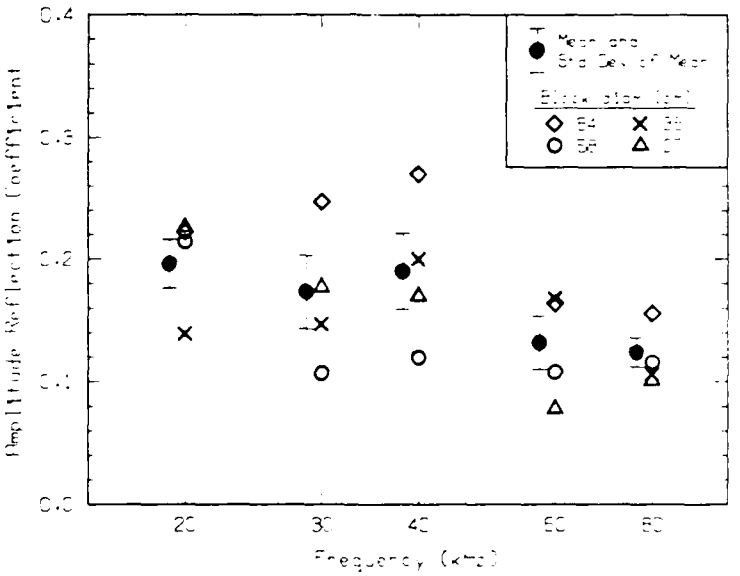

Figure 41. Average reflectivity of the skeletal layer for the four block diameters, showing a decrease with frequency.

B. Effect of Submergence

Two of the blocks were kept submerged long enough for repeat measurements. Runs 3 and 4 were made 22 hours apart on the 84-cm block, followed by three spot checks during the next 6 hours. The change in reflectivity with time is shown in Figure 42 (left). The target strengths of the calibration sphere are shown to indicate any equipment changes. The target strength of the ice block reflection decreased considerably during the 22 hours between Runs 3 and 4, the more so the higher the frequency.

To learn more about the change in reflectivity with time, the reflection was monitored at close intervals for 15 hours after the next measurement, Run 5 with the 58-cm block. The target strengths are plotted in Figure 42 (right). A correction of +6.4 dB has been applied to the 58-cm block data for area normalization. The sphere returns show that the equipment varied for three of the pings; thus the corresponding variations in the ice block return can be ignored. (This variation illustrates the importance of monitoring a calibration target on every ping.) The reflections decreased with time, by as much as 9 dB at 80 kHz, where the reflectivity would be the most sensitive to small variations in the surface or in the skeletal layer.

Figure 43 compares the normal-incidence reflectivity changes in the two blocks during several hours of submergence. At 20 kHz the effect of prolonged submergence was small for both blocks. At 30 kHz and above, there was a large change for the 84-cm block and a small change for the 58-cm block. It appears that an appreciable change takes place in the skeletal layer in the first 24 hours of submergence.

We are not sure exactly how long each block was submerged before its reflection was first measured. Assuming equal delays, we have superimposed on Figure 44 the two plots of Figure 42. It is apparent that the higher the frequency, the greater the effect of warming. Otherwise, the changes in the two blocks do not seem to follow the same evolution.

What changes would take place during preparation of the block? When a block is cored out, the melt water warms the block around the perimeter. After the block is forced down 1 m, it continues to be warmed from the outside by the surrounding −1.7°C water. Specifically, the skeletal layer remains at the same temperature while the transition zone is warming. Equilibrium between brine and ice would require some melting of the ice surrounding the brine pockets, even to the extent of producing drainage holes through the bottom. This would roughen the bottom surface and decrease the

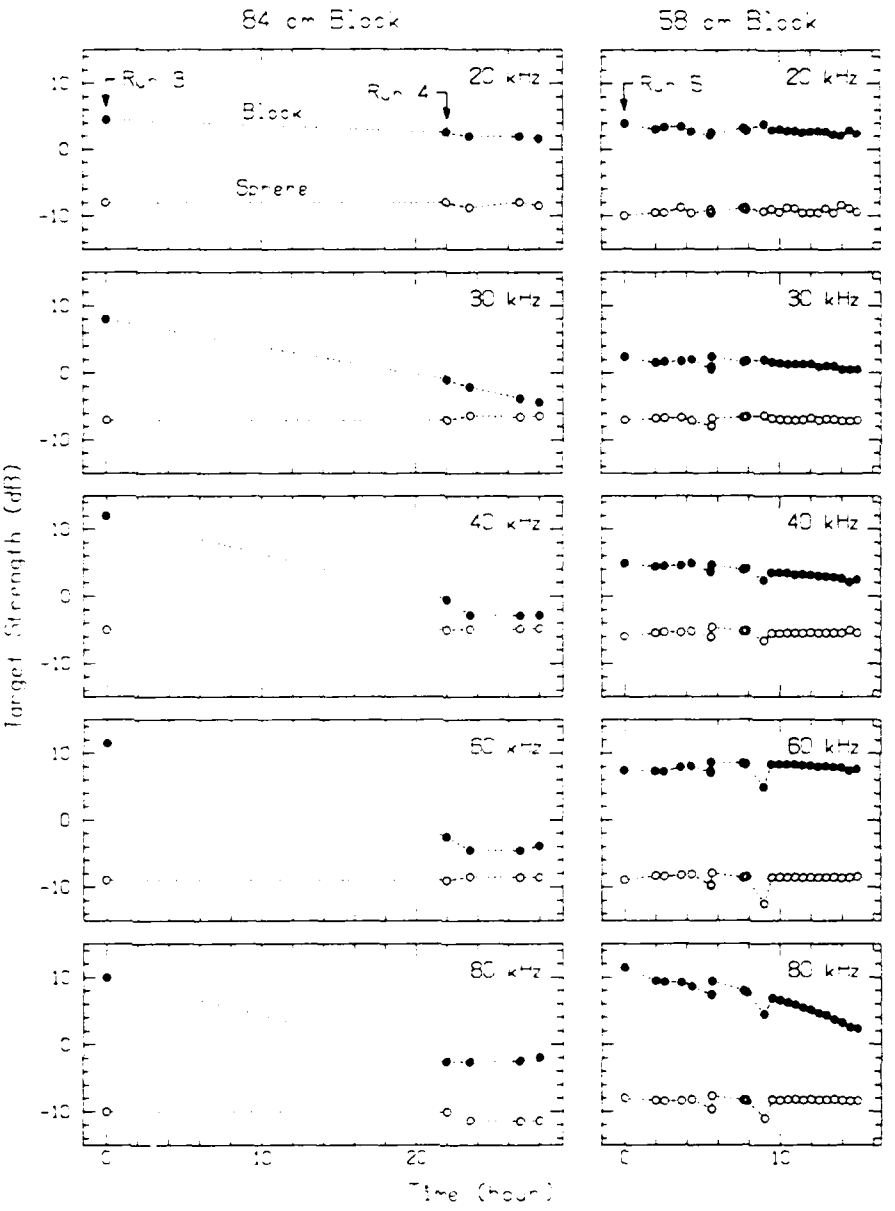

Figure 42. Changes in the returns from two submerged ice blocks with time. The data for the 58-cm block have been adjusted by +6.4 dB for area normalization. Changes observed after 22–28 hours in the 84-cm block (left) led to a 15-hour monitoring of the 58-cm block (right).

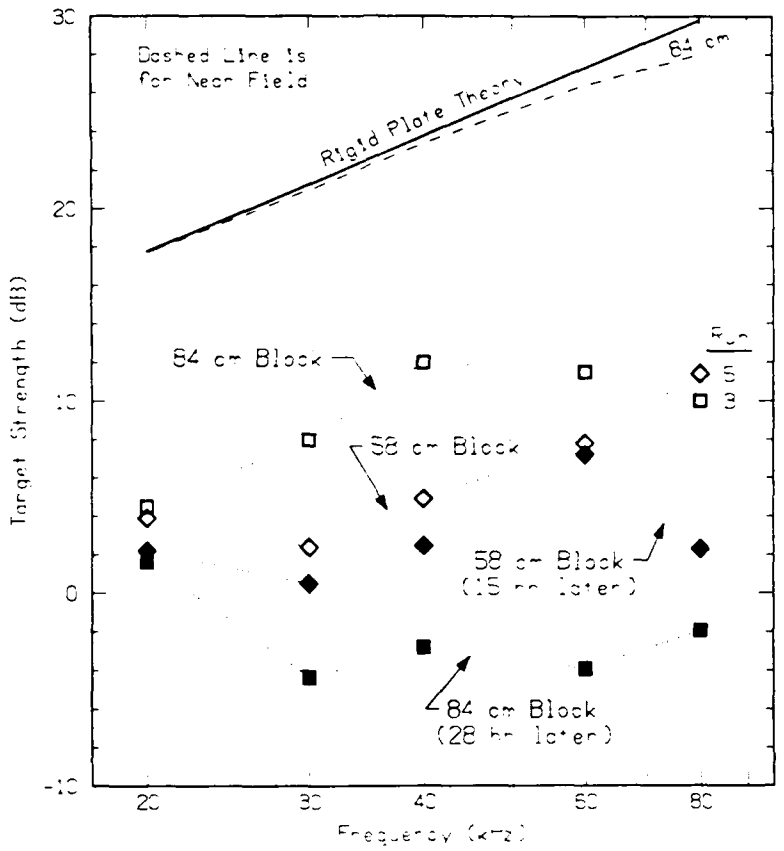

Figure 43. Changes in the returns at normal incidence from the 58-cm and 84-cm blocks after several hours of submergence. The data have been normalized for area.

reflection. Such holes were not noticed when the blocks were removed and inverted for the flatness measurement, but some shallow, thumb-sized depressions did appear after a few hours.

C. Skeletal Layer Modifications

To determine the effect of the skeletal layer on acoustic reflection, we wanted to remove thin layers successively from the bottom of the block and measure the reflection after each removal. With no means of cutting off the block under water, we had to remove it. Withdrawing the block into the air would, of course, allow the skeletal layer to drain and cool, causing some freezing, and these changes would extend into the portion of the transition zone remaining after the saw cut. When the block was replaced in the hole, the reflections would probably be enhanced by the air trapped in the remaining transition zone and by the additional freezing.

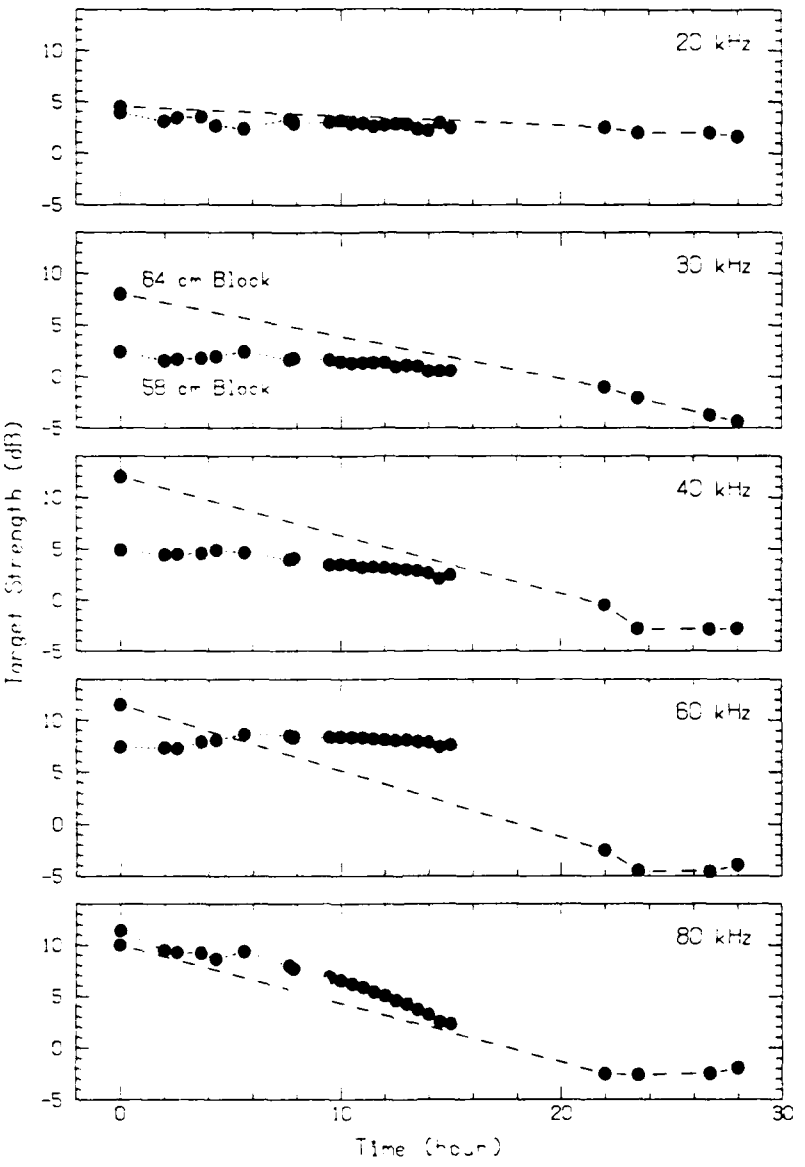

Figure 44. A comparison of the two time series. The data have been normalized for area. The effect of warming appears to be greater the higher the frequency.

We attempted to avoid these problems by placing insulation around the skeletal layer and transition zone at the lower end of the block as we removed it from the hole and by inverting the block to allow trapped air to escape when it was again submerged. The insulating procedure went well, but turning the block over was difficult because of the current.

To review briefly, (1) a 58-cm diameter block was cut from natural ice, lowered into position, and the reflections measured (Run 5, Figure 29); (2) the block was then raised, insulated, drained, and relowered (Run 6, Figure 34, showing increased reflectivity); (3) the block was raised, insulated, and the top cut off; (4) the block was relowered with the skeletal layer up to let air escape, turned over under water to place the skeletal layer downward, and forced down with the air cylinder over the top (Run 7, Figure 36, showing increased reflectivity with a good pattern). A direct comparison of the target strengths at normal incidence for these various modifications is shown in Figure 45.

When we raised the 58-cm block out of the water while keeping the lower end insulated and let it drain for 40 minutes before resubmerging, the reflection increased 6–8 dB at the lower three frequencies (Run 6, Figure 34). Apparently, the skeletal layer had either retained trapped air or frozen so that it gave a high reflection. Examination of the phase of the return showed it to be about the same as the phase for the air block return, indicating the high reflection was caused by trapped air. In any case, removal of a block for a half-hour or so greatly increased the reflective properties of the skeletal layer.

When we removed the block again and sawed off the top, the reflections from the skeletal layer at the lower frequencies increased to a level only 7 dB below the theoretical return for a rigid plate (Run 7, Figure 36). This might result if the skeletal surface froze solid with a sound speed of 4200 m/s. This is considerably higher than any of our sound speed measurements; thus we turn to an alternate explanation—sufficient air was trapped in the skeletal layer to make it respond more like a pressure release surface. Again, the phase of the return indicated the presence of trapped air.

To obtain a solid ice face for comparison, our final experiment consisted of sawing the ends off an ice block that had been in the air for 4 days, positioning it in the hole, and measuring the reflections from the lower face. The result was a high reflection (Run 14, Figure 38), except for a falloff at the higher frequencies. This falloff could be related to a curved or rough saw cut which would have a greater effect at the shorter wavelengths. The phase of the return was the same as for the air-water interface, a disturbing result as we saw no indication of trapped air. This anomaly is being investigated further.

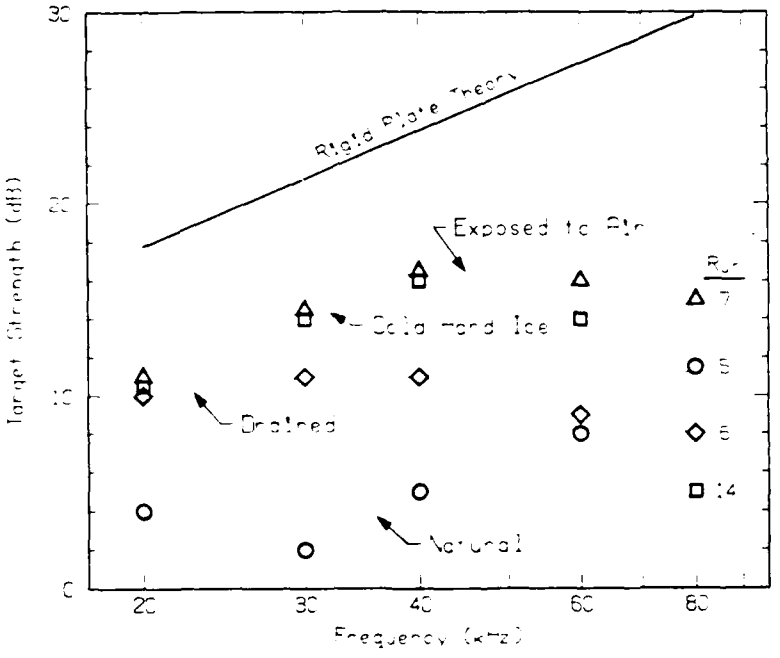

Figure 45. Target strength measurements at normal incidence of the 58-cm block after several modifications. The data have been normalized for area.

VII. UPPER FACE REFLECTIONS AND ABSORPTION

Reflections recorded from the upper surface in 1986 gave some measure of the absorption in the ice. However, we suspect that most of the absorption takes place in the skeletal layer and transition zone. In 1988 we added an air space above the sawed-off blocks to increase the amplitude of the upper-face reflection. Despite this, we observed few reflections from the upper face. Perhaps the reflection from the lower face was higher than in 1986 and less energy passed through the blocks.

For blocks with snow covering the upper surface, the internal reflection off the upper face is unpredictable, especially for a block that has been submerged for an hour or so. We were unable to detect any upper-face reflections for the uncut ice blocks.

For the sawed-off blocks with air above, some reflections from the upper face were measurable. To calculate absorption in the ice, we treat the sound as a plane wave striking an infinite surface. At the lower surface, the transmitted sound has an amplitude of $(1 + R_a)$ times the incident amplitude, where R_a is the reflection coefficient of the lower face. Upon reflection from the upper face, the amplitude changes by a factor of R_b, the reflection coefficient of the upper face, which is negative in this instance. As the sound passes through the lower face, the amplitude changes by a factor of $(1 - R_a)$. Absorption occurs both ways. The measured amplitudes should therefore follow the relationship

$$20 \log (A_2/A_1) = 20 \log (1+R_a) + 20 \log (1-R_a) + 20 \log (-R_b) - 20 \log R_a - 2\alpha t \ , \quad (2)$$

where t is the thickness, α is the absorption coefficient, and A_1 and A_2 are the amplitudes of the returns from the lower and back faces, respectively. We solve Eq. 2 for the absorption coefficient to obtain

$$\alpha = \frac{1}{2t}\left\{20 \log \left[\frac{1-R_a^2}{R_a}\frac{A_1}{A_2}(-R_b)\right]\right\}. \quad (3)$$

If $R_b = -1$, we have

$$\alpha = \frac{1}{2t}\left\{20 \log \left[\frac{1-R_a^2}{R_a}\frac{A_1}{A_2}\right]\right\}. \quad (4)$$

A reflection from the upper face was observed on the 58-cm diameter block with the upper portion sawed off and an air layer above. Figures 46 and 47 show the reflections at

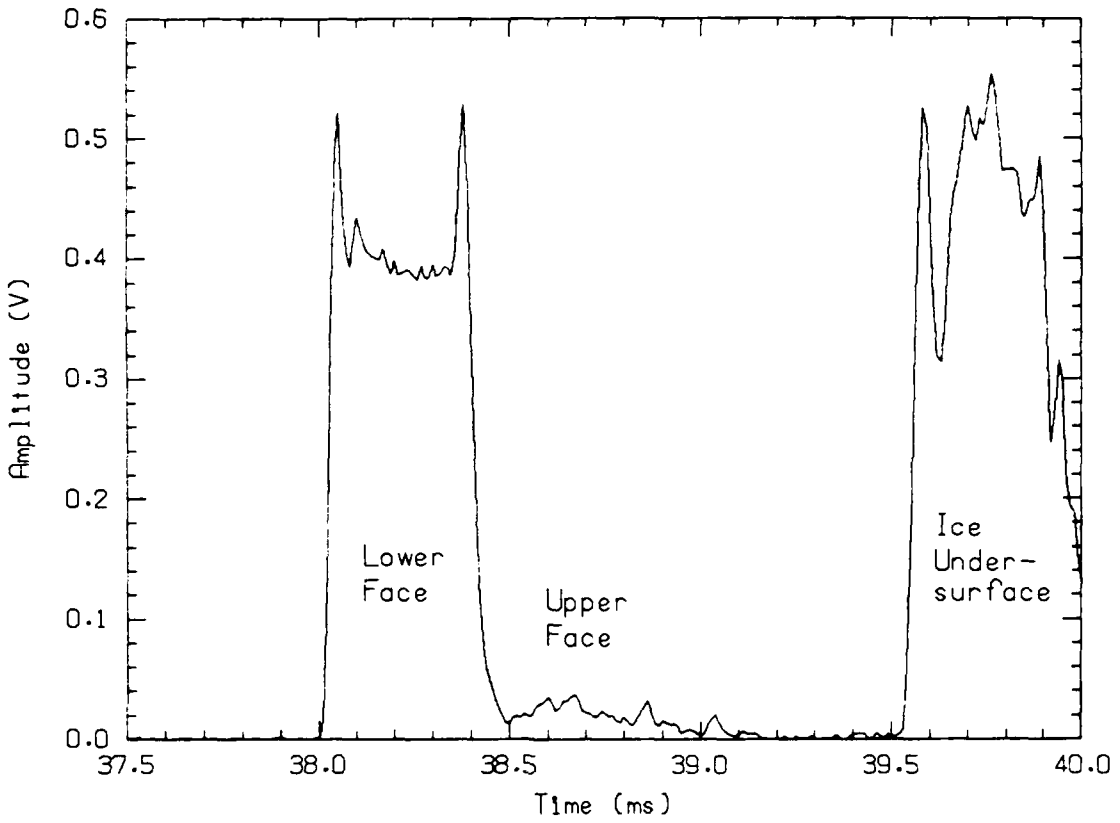

Figure 46. Return from the 58-cm ice block with the upper end sawed off. The reflection from the lower face of the block is followed by a weak reflection from the upper face. Run 7, 30 kHz.

30 and 80 kHz for Run 7. The delay between the reflections from the lower and upper faces appears to be 0.50 ms. The block was 87 cm long, so the average sound speed in the ice would be 3480 m/s.

For this block, which had a sawed-off top and a natural bottom, the reflection from the natural lower face at 30 kHz was 7 dB below the theoretical value (Figure 36) and corresponds to $R_a = 0.45$. The measured amplitudes in Figure 46 are 0.4 V for A_1 and 0.04 V for A_2. Using Eq. 3, we calculate an absorption loss of 12 dB each way through the ice, or an absorption coefficient of 14 dB/m for uniform absorption in the ice.

The measured absorption coefficient of 14 dB/m is much higher than that predicted from the relationship between ice absorption and temperature derived by McCammon and McDaniel[5] for ice without a skeletal zone, indicating that the upper surface did not reflect perfectly or that the skeletal layer and transition zone produced a major part of the absorption.

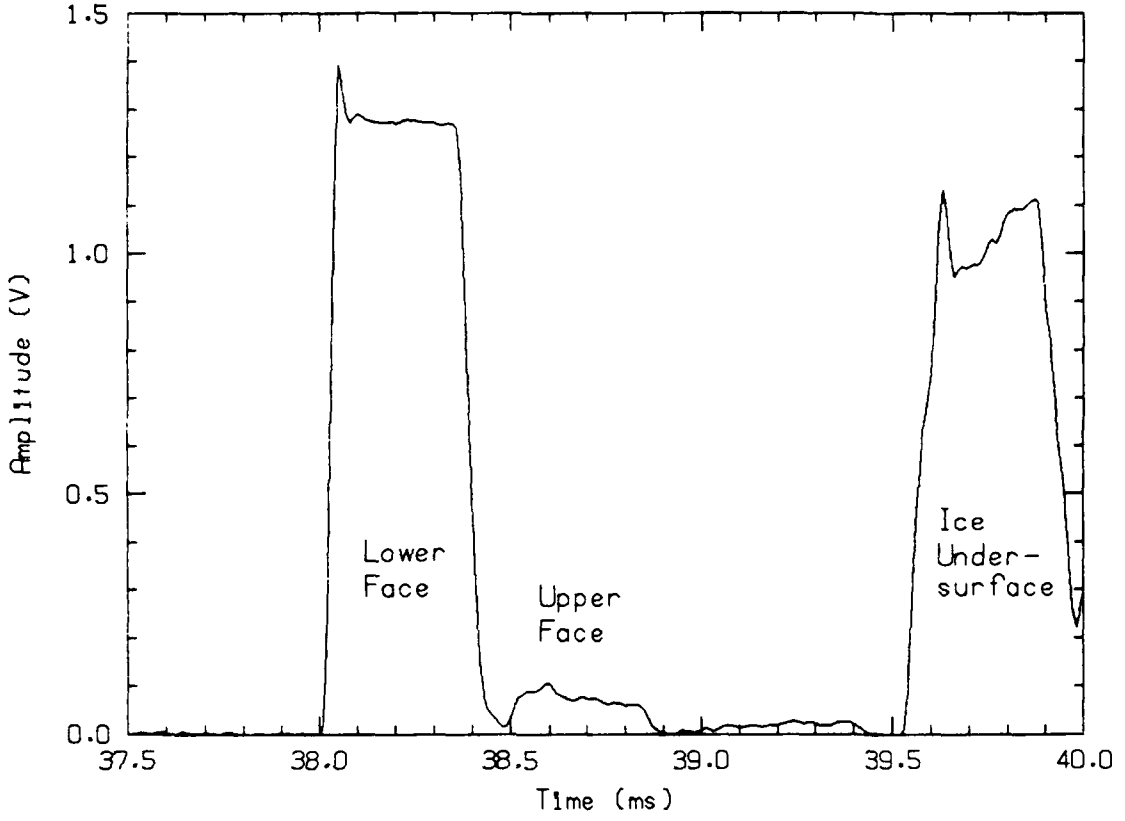

Figure 47. Return from the 58-cm ice block with the upper end sawed off, showing the reflections from the lower and upper faces. Run 7, 80 kHz.

The absorption coefficient calculated from the upper face reflection shown in Figure 47 for the same block at 80 kHz is 18 dB/m, in good agreement with the 14 dB/m calculated for 30 kHz but still unreasonably high. The returns shown in Figure 48 for a block sawed off at both ends give an even higher absorption, indicating that it is not high absorption in the transition zone, but rather an increased absorption in the ice or a lower-than-expected reflection from the upper face, that causes the calculated absorption to be so high. We had assumed that the upper face, a sawed-off interface between ice and air, would have a reflection coefficient of unity, but perhaps the ice was not flat enough.

The reflections from the aluminum pan filled with water are shown in Figure 12 (p. 15). If we use a sound speed ratio of 4.46 between aluminum and water (6420 m/s vs 1440 m/s) and a density ratio of 2.7, the impedance ratio is 12.0. The reflection coefficient calculated for normal incidence is $(12.0-1)/(12.0+1)$, or 0.85; i.e., 1.4 dB

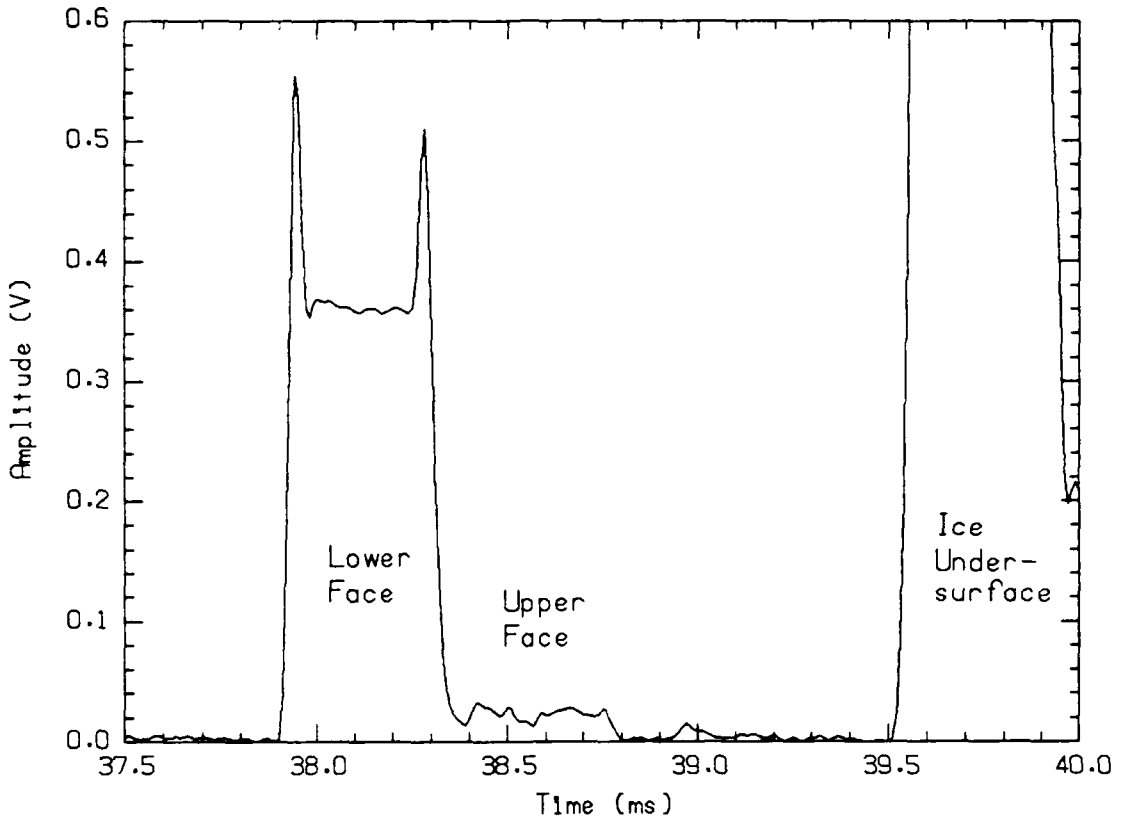

Figure 48. Return showing lower and upper face reflections from the 58-cm diameter ice block that had been in the cold air for 4 days and then had both ends sawed off. Run 14, 80 kHz.

below the theoretical return from an air-water interface. However, the calculation should include the multiple reflections from the upper face of the 3.2-mm thick aluminum. This was done in a detailed calculation by applying equations developed by Clay and Medwin[6] to a thin layer of aluminum with seawater above and below. The calculated results are shown in Figure 49 and compared with our measured values, which are the scaled differences between the theoretical curves and the measurements shown in Figure 12. The theory predicts a reflection loss varying from −9 dB at 20 kHz to −2 dB at 80 kHz, and the measurements were only about 2 dB lower. Some examples given in Ref. 6 had several oscillations; for this thickness of aluminum, however, the reflection is predicted to increase with frequency to a maximum at 500 kHz.

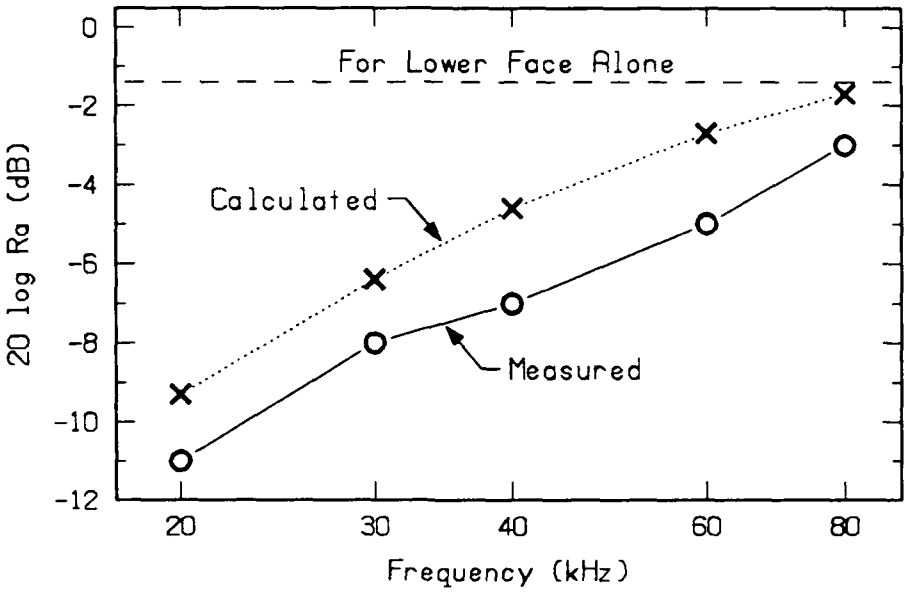

Figure 49. Reflections from a thin layer (3.2 mm) of aluminum immersed in seawater, with multiple internal reflections included.

VIII. TOPOGRAPHY OF UNDER-ICE SURFACE

A. Undulations

Refrozen leads generally appear very flat and level, at least to an observer on the ice. Some snow is usually present which may vary in depth, especially near the edges of the lead. For an observer below the ice, variations in ice thickness are more easily seen, despite the poorer visibility, because of refraction effects. Under-ice profiles made with a shallow depth, slowly moving, high-frequency profiler[7] show there are often undulations which appear nearly sinusoidal in section. These may be due to windrowing which varies the insulating effect of the snow and causes variations in the freezing rate at the lower surface of the ice.

A scan of the surrounding area with an underwater TV camera placed beneath the lead near one of the ice blocks showed what appeared to be undulations oriented in one direction. After all the block reflections were measured, divers stretched a taut line beneath the ice and measured the offset of the ice from the line at 1 m increments. The results are plotted in Figure 50 along with the best-fit sine wave, which shows a wavelength of 8.5 m and an amplitude of 3.7 cm.

Using our numerical integration method, we calculated the effect of these undulations on an 84-cm block cut from the portion of the sine wave with a maximum rate of change in slope, and thus having maximum effect on the reflection at normal incidence. The effect was less than 1 dB and would be even less for the smaller blocks. Thus undulations of this size are not an important factor in the reflection measurements.

B. Flat Plate Reference

Prior to the field trip, some rigid flat aluminum plates, about 3.2 mm thick and the same diameter as the ice blocks, were prepared as references to measure the flatness of the ice surface. Holes were drilled in the plates over an x-y grid, and a probe was inserted through the holes to measure the deviation between the plate and the ice. Three short legs held the plate away from the ice block, which had been brought onto the surface and inverted.

The results are shown in Figure 51. The standard deviations, rounded to one decimal place, are 1.0, 1.1, 2.7, and 3.1 mm for the 27, 38, 58, and 84 cm blocks, respectively. There is some indication of a sloughing off at the edges of the block, which might have made the effective diameter smaller for the block reflection measurements.

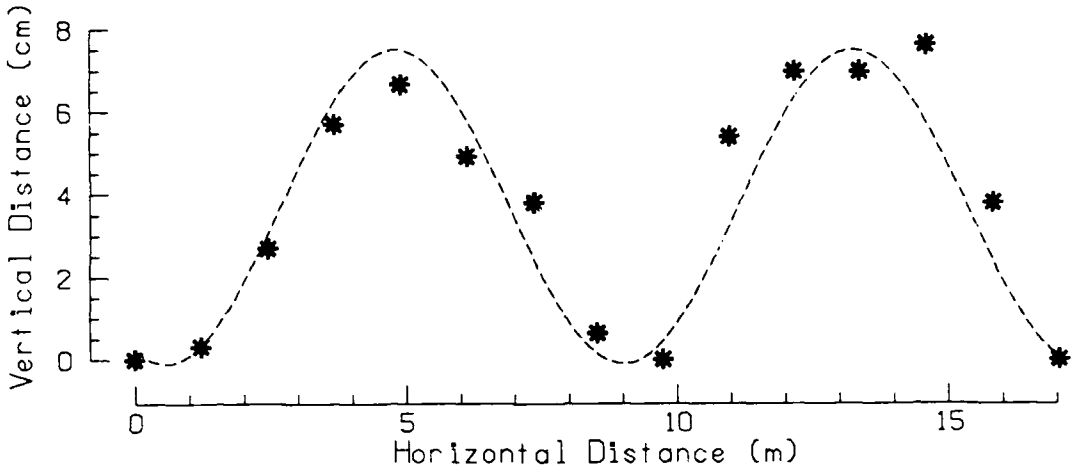

Figure 50. Measured undulations in the area of the ice block experiment. A sine curve has been fitted to the data.

The largest variation (ignoring the sloughing at the edges) is about 3 mm, or 1/6 of a wavelength at 80 kHz. A change in range of 1/6 wavelength would cause the phase of the return to vary by 120°, reducing the sum for some contributions by 50%. The results of such roughness, estimated by numerical integration combined with Monte Carlo selection, are shown in Figure A1 of Ref. 2. For the 84-cm block at 80 kHz, the effect can be as much as 18 dB. The reflection measurements for the 84-cm block show a small drop-off at 80 kHz (about 6 dB), about like that predicted for a standard deviation of 2 mm. This suggests that the measured roughness may be the cause of the reduced reflectivity at 80 kHz, but further analysis is needed.

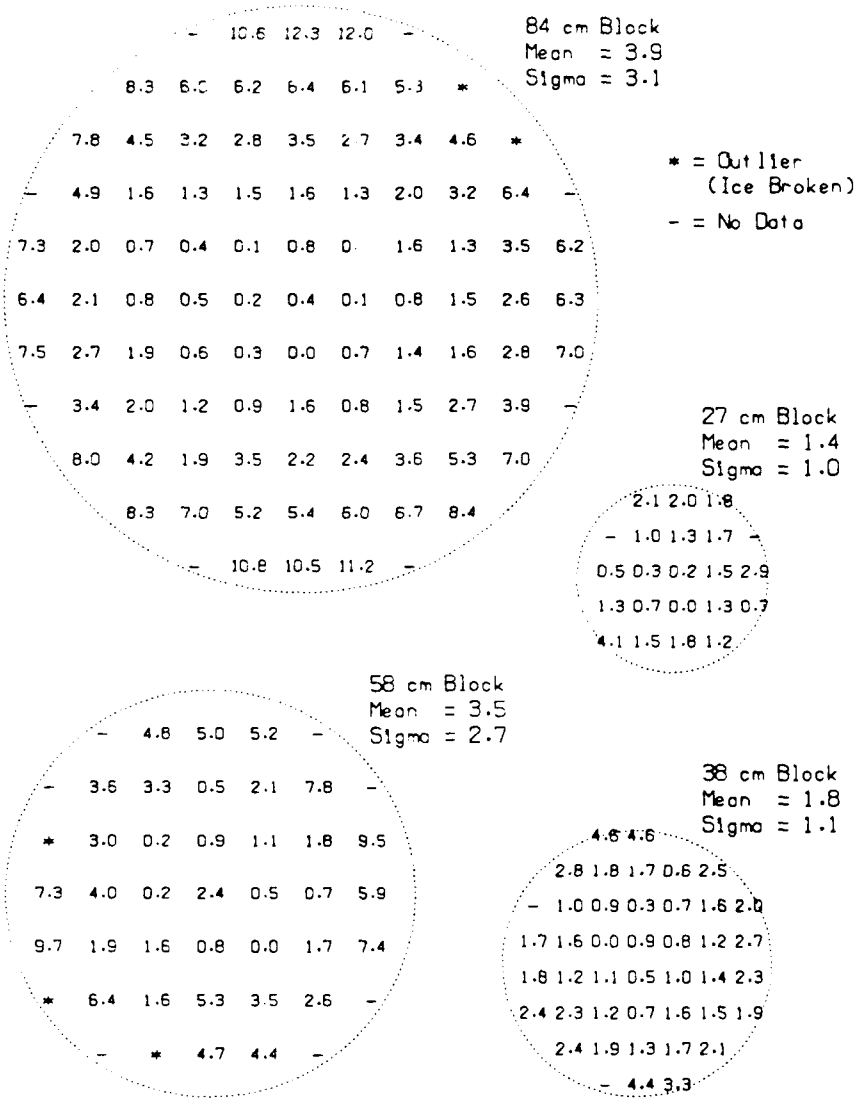

Figure 51. Deviations (mm) of the ice block surfaces from a plane, in this case, a flat aluminum plate.

IX. ICE AND WATER PROPERTIES

The environment at the 1988 ice camp is described in detail in Ref. 3. Those properties most directly related to the ice block experiment are summarized here.

A. Effect of Snow

Additional information on the temperature distribution in the ice was obtained by measuring the surface temperature of the ice at various locations around the camp. This was accomplished by drilling a small-diameter hole about 4 cm deep in the ice and inserting a thermocouple probe. The surface temperature varied greatly, depending on the amount of loose snow cover, from −14°C where there was good insulation to −24°C (the air temperature) where the ice was bare.

The temperature of ice generally varies uniformly with depth, with a gentler gradient when snow is present. This probably has some effect on the configuration of the skeletal layer and transition zone. The brine pockets between the ice platelets tend to close off at a given temperature, and the steeper the temperature gradient, the nearer the bottom this temperature will occur.

B. Ice Cores

During the experiment, two ice cores were taken within 10 m of the ice block area, one on 25 March and one on 3 April. The measured temperature, salinity, and density profiles are shown in Figures 52 and 53, along with the calculated brine volume and sound speed. We attempted to obtain samples at several levels within the skeletal transition zone. However, this ice is crumbly and difficult to sample, and the temperature and density were difficult to measure. The salinity of the transition zone, though measured accurately, was altered by brine drainage as the core was removed. The snow in the vicinity of the ice blocks was somewhat trampled, and thus the ice was probably colder than where the ice cores were taken.

The ratio of brine volume v to salinity S was calculated using the relationship developed by Frankenstein and Garner[8] for three ranges of ice temperature:

$$\begin{aligned} v &= S(-52.56/T - 2.28) \qquad (-2.06 \text{ to } -0.5°C) \\ v &= S(-45.917/T + 0.93) \qquad (-8.2 \text{ to } -2.06°C) \\ v &= S(-43.795/T + 1.189) \qquad (-22.9 \text{ to } -8.2°C) . \end{aligned} \tag{5}$$

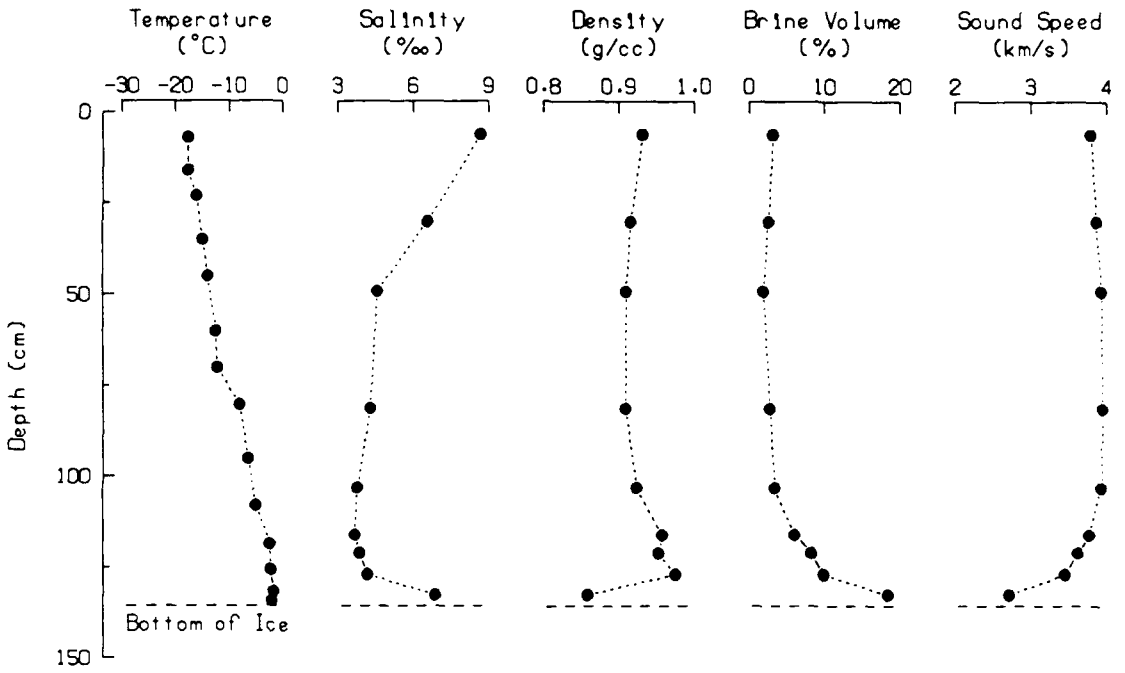

Figure 52. Measured temperature, salinity, and density profiles for an ice core taken on 25 March 1988. The brine volume and sound speed have been computed and added. The bottommost sample consisted of the ice remaining after brine drainage; thus the values shown for this sample are not applicable.

These equations would not be applicable to a porous skeletal transition zone.

The modulus of elasticity E can be estimated from the brine volume[9] by

$$E = (10.00 - 0.0351v) \times 10^{10} \quad [\text{dynes/cm}^2] \,. \tag{6}$$

The sound speed can be related to E and Poisson's ratio μ by[10]

$$c = \{(E/\rho)[(1-\mu)/(1+\mu)(1-2\mu)]\}^{1/2}/100 \quad [\text{m/s}] \,, \tag{7}$$

where ρ is the density and μ is approximately 0.35.

Although the computation of brine volume for the sample near the bottom of the core is questionable, some direct measurements of the sound speed in neighboring ice also indicated a dropoff near the bottom of the ice. A gradual change in sound speed near the bottom would reduce the reflection compared with that for an abrupt change.

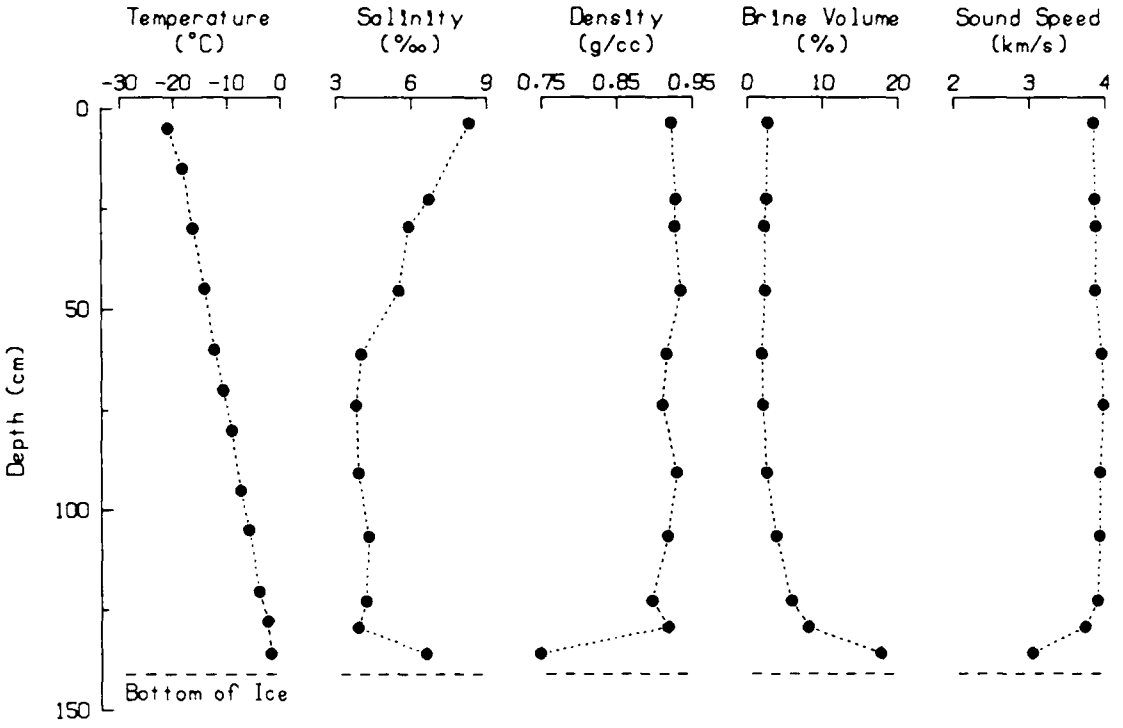

Figure 53. Measured temperature, salinity, and density profiles for an ice core taken on 3 April 1988. The brine volume and sound speed have been computed and added. The bottommost sample consisted of the ice remaining after brine drainage; thus the values shown for this sample are not applicable.

C. CTD Profiles

The water properties just below the ice can be obtained from CTD profiles[3] taken at the hut 100 m away. The mixed layer near the surface generally had a temperature of −1.71°C and a salinity of 31.5 ppt. The freezing temperature of water with this salinity is −1.73°C. With these conditions, it is easy to assume that freezing was taking place continually at the bottom surface of the ice, where the temperature could very well have been 0.02° colder than in the mixed layer.

D. Weather

In estimating the thickness of the ice at a particular location, it is important to know the temperature history for the previous weeks. In our case, weather records at the ice camp, plus ones taken earlier during the search for a suitable floe, were helpful in analyzing the growth rates of the ice. Plots of the weather data are shown in Figure 54. The air

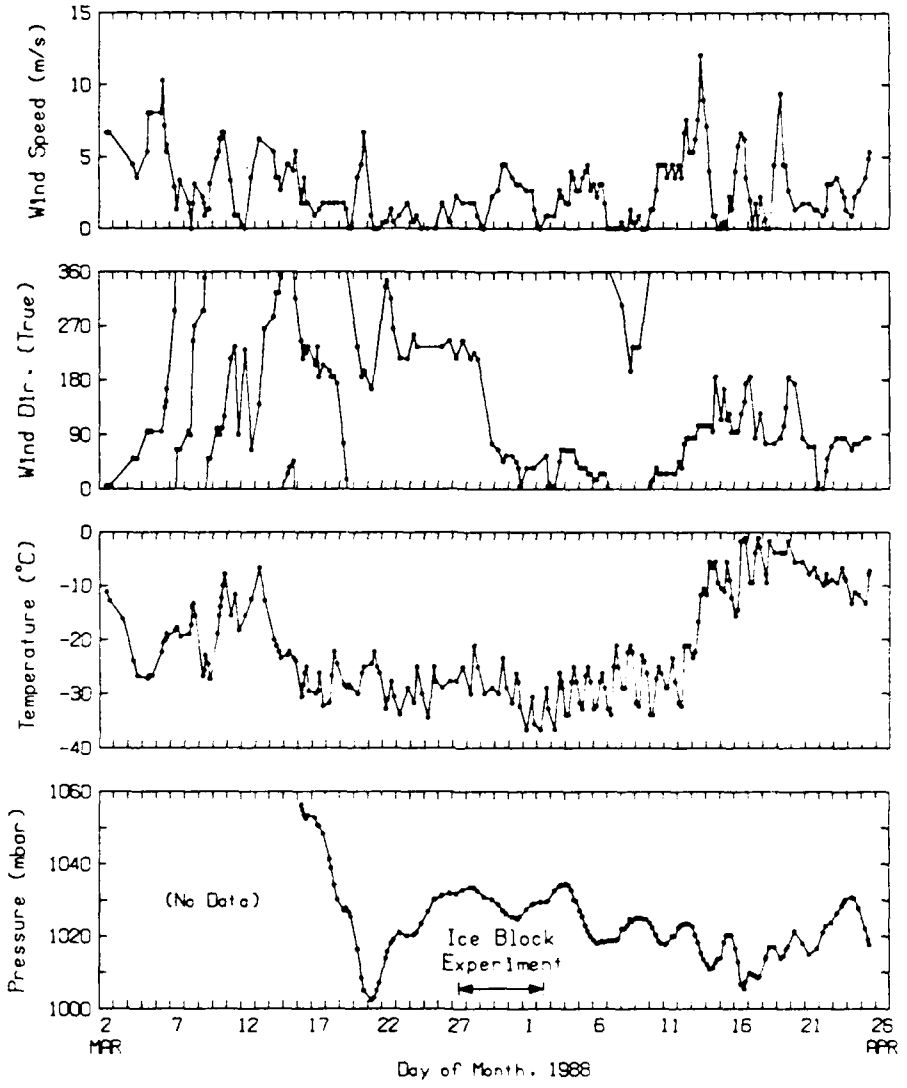

Figure 54. Weather records at the 1988 ice camp. The ice blocks were measured during 27–30 March. The modified ice blocks were measured through 2 April.

temperature had been fairly steady for 2 weeks prior to the experiment except for a diurnal variation of 8°C. The wind speed was usually about 3 m/s with a maximum of 5 m/s (10 knots). The floe drift, as measured from NAVSAT data, was minimal during this period.

X. DISCUSSION AND RECOMMENDATIONS

A. Discussion

Low Reflectivity of Skeletal Layer

The target strength of the ice block face measured 8–11 dB lower when a skeletal layer was present. A plausible explanation for the low reflectivity of the skeletal layer is that the acoustic impedance is lower than in solid ice, so the water-ice impedance mismatch is less abrupt and produces lower reflections.

Two factors affect the acoustic impedance—density and sound speed. The deepest sample taken from the 3 April ice core had a measured density of 0.75. We know that the density of the transition zone, which is a combination of pure ice and trapped brine that is concentrated as a result of the freezing process, should always (in the absence of gas bubble voids) be greater than 0.918, the approximate density of pure ice alone at its freezing temperature. Therefore the low density measured is undoubtedly due to brine drainage from the sample when it was removed during coring and indicates there were open pores in the skeletal layer and transition zone. The high salinity indicates there are also closed, brine-filled pores. As a result, the in situ density, when all pores are filled with seawater or brine, would tend to be higher than in the solid ice above. Another consideration is that the effective density of the skeletal layer and transition zone, for acoustic purposes, may be lower in situ because of the way the brine in the pores is dynamically coupled to the ice and seawater. The question of the effective density near the interface remains to be answered.

The more important factor affecting the impedance in the skeletal transition zone is the sound speed c, which depends on the modulus of elasticity E of the medium and the density ρ, i.e., $c \propto \sqrt{(E/\rho)}$. The porosity in the transition zone reduces E; since ρ is about the same as in the ice above, the calculated sound speed is lower. For example, the lowest sample from the 3 April ice core (Figure 53) had a calculated sound speed of 2810 m/s, based on the measured density of 0.75. If we assume that, instead, the in situ bulk density in the skeletal layer was 0.92, the same as in the sample just above it, the calculated sound speed would be even lower, 2742 m/s. These values for density and sound speed would give an impedance ratio of 1.71 between the transition zone and the

water. This corresponds to a plane wave reflection coefficient of 0.26, which is still higher than the reflection coefficients measured here for all blocks (Figure 41).

Perhaps the predicted reflectivity would be lower if we included reflections from several successive impedance changes within the ice, along with their various phase offsets. A study of the effect of a gradual transition in sound speed has been made by Mourad,[11] who found that a sound speed profile similar to that observed here would result in a reflection coefficient with a frequency dependence similar to that measured for the under-ice surface.

Changes in Reflectivity

The reflectivity of a block face with a skeletal layer decreased with time when the block was cored out and forced down into the water. The change is apparently related to the temperature increase produced in the skeletal transition zone by submergence in the water, which is much warmer. (In this regard, we note that cooling of the block in air always resulted in a higher reflectivity.) Further study should be made of these changes in the skeletal transition zone with temperature, and the accompanying change in reflectivity, to obtain a better understanding of the skeletal layer and the transition to solid ice. With such knowledge we may be able to predict the reflectivity of ice blocks in various keel formations.

Importance of Skeletal Layer to Study of Ice Keel Reflections

How important are skeletal layer reflections to the study of ice keel reflections? Although the original skeletal layer is present on only one-sixth of the faces of rectangular blocks, the cleavage faces tend to be smaller than the top and bottom faces; as a result, many of the largest and flattest faces will have a skeletal layer. Also, a skeletal layer of some sort may form on all surfaces of a very cold block after it is submerged during ridge formation.

B. Recommendations

Future work should include a more detailed examination of the physical and acoustic properties of the skeletal layer and transition zone. What are the seasonal variations

in the reflectivity, and how are they related to observable properties of the layer? Many reflection measurements are needed—more than can be efficiently obtained from cored-out ice blocks. An acoustic beam directed against the undersurface, possibly with the transducer carried by divers or on a small submersible, is recommended, along with numerous ice cores, to study the relationship between acoustic reflectivity and the physical properties of the skeletal layer and transition zone.

Laboratory measurements involving full-scale, thick sea ice under controlled conditions would be very helpful in resolving the intrinsic acoustic transmission and reflection characteristics. Field measurements will yield more accurate information on the surface condition of the ice that contributes to its reflection/scattering signature. A combination of both laboratory and field measurements would be extremely profitable in promoting a satisfactory understanding of the mechanisms involved for use in advanced modeling of sea ice response at high frequency.

XI. REFERENCES

1. G.R. Garrison, R.E. Francois, T. Wen, and R.P. Stein, "Measurements of acoustic reflection from the end of a cylindrical block of arctic ice," APL-UW 8506, Applied Physics Laboratory, University of Washington, Seattle, September 1986.

2. G.R. Garrison, R.E. Francois, T. Wen, and R.P. Stein, "Acoustic reflections from cylindrical blocks of arctic ice, 1986," APL-UW 8707, Applied Physics Laboratory, University of Washington, Seattle, August 1988.

3. T. Wen, W.J. Felton, J.C. Luby, W.L.J. Fox, and K.L. Kientz, "Environmental measurements in the Beaufort Sea, Spring 1988," APL-UW TR 8822, Applied Physics Laboratory, University of Washington, Seattle, March 1989.

4. R.J. Urick, *Principles of Underwater Sound* (McGraw-Hill, New York, 1975), p. 275.

5. D.F. McCammon and S.T. McDaniel, "The influence of the physical properties of ice on reflectivity," *J. Acoust. Soc. Am.* 77, 499–507 (1985).

6. C.S. Clay and H. Medwin, *Acoustical Oceanography: Principles and Applications* (John Wiley and Sons, New York, 1977), p. 66.

7. R.E. Francois and W.E. Nodland, "Arctic acoustic measurements at 50 kHz," APL-UW 7313, Applied Physics Laboratory, University of Washington, Seattle, August 1973.

8. G. Frankenstein and R. Garner, "Equations for determining the brine volume of sea ice from −0.5 to −22.9°C," *J. Glaciology* 6, 943–944, 1967.

9. G.F.N. Cox and W.F. Weeks, "On the profile properties of undeformed first-year sea ice," CRREL special report, presented at 2nd Ice Penetration Technology Workshop, 16–19 June 1986, at Monterey, California.

10. E. U. Condon and H. Odishaw (Eds.), *Handbook of Physics*, 2nd Ed. (McGraw-Hill, New York, 1989), p. 399.

11. R. E. Francois, K. L. Williams, G. R. Garrison, P. D. Mourad, and T. Wen, "Ice keels I: Intrinsic physical/acoustic properties of sea ice and scattering from ice surfaces," *U. S. Navy J. Underwater Acoustics* (in press).

UNCLASSIFIED

SECURITY CLASSIFICATION OF THIS PAGE

REPORT DOCUMENTATION PAGE

Form Approved
OMB No 0704-0188

1a REPORT SECURITY CLASSIFICATION
Unclassified

1b RESTRICTIVE MARKINGS

2a SECURITY CLASSIFICATION AUTHORITY

2b DECLASSIFICATION DOWNGRADING SCHEDULE

3 DISTRIBUTION AVAILABILITY OF REPORT
Approved for public release; distribution is unlimited.

4 PERFORMING ORGANIZATION REPORT NUMBER(S)
APL-UW TR 8815

5 MONITORING ORGANIZATION REPORT NUMBER(S)

6a NAME OF PERFORMING ORGANIZATION
Applied Physics Laboratory
University of Washington

6b OFFICE SYMBOL (If applicable)

7a NAME OF MONITORING ORGANIZATION
Naval Oceanographic and Atmospheric Research Laboratory

6c ADDRESS (City, State, and ZIP Code)
1013 N.E. 40th Street
Seattle, WA 98105-6698

7b ADDRESS (City, State, and ZIP Code)
Stennis Space Center, MS 39529-5004

8a NAME OF FUNDING SPONSORING ORGANIZATION
Office of Naval Technology

8b OFFICE SYMBOL (If applicable)

9 PROCUREMENT INSTRUMENT IDENTIFICATION NUMBER
SPAWAR N00039-88-C-0054

8c ADDRESS (City, State, and ZIP Code)
Ballston Center, Tower #1
800 N. Quincy St., Arlington, VA 22217

10 SOURCE OF FUNDING NUMBERS

PROGRAM ELEMENT NO	PROJECT NO	TASK NO	WORK UNIT ACCESSION NO

11 TITLE (Include Security Classification)
Acoustic Reflections from Cylindrical Blocks of Arctic Ice, 1988

12 PERSONAL AUTHOR(S)
G.R. Garrison, R.E. Francois, T. Wen, and W.J. Felton

13a TYPE OF REPORT	13b TIME COVERED	14 DATE OF REPORT (Year Month, Day)	15 PAGE COUNT
Technical	FROM 2/18/88 TO 3/8/88	January 1990	77

16 SUPPLEMENTARY NOTATION

17 COSATI CODES			18 SUBJECT TERMS (Continue on reverse if necessary and identify by block number)
FIELD	GROUP	SUB-GROUP	Arctic ice; Acoustic reflection from ice; Ice properties
20	01		
15	06	02	

19 ABSTRACT (Continue on reverse if necessary and identify by block number)

In spring 1988 acoustic reflections were measured from the submerged ends of cylindrical blocks of arctic ice, in an extension of similar efforts in 1984 and 1986. Blocks with diameters of 27, 38, 58, and 84 cm were individually depressed below the surface of the ice floe so that reflections from the bottoms of the blocks were separable from those off the underside of the ice canopy. The source/receiver was moved horizontally beneath the block to measure the angular response pattern. Measurements to determine the effect of the so-called skeletal layer showed that compared with solid ice the layer reduced the reflection at normal incidence by 8-11 dB in the frequency range 20-80 kHz for all blocks. Properties of the skeletal layer and the transition zone were also measured to study the nature of the reflection.

20 DISTRIBUTION AVAILABILITY OF ABSTRACT
☐ UNCLASSIFIED/UNLIMITED ☒ SAME AS RPT ☐ DTIC USERS

21 ABSTRACT SECURITY CLASSIFICATION
Unclassified

22a NAME OF RESPONSIBLE INDIVIDUAL	22b TELEPHONE (Include Area Code)	22c OFFICE SYMBOL
Robert W. Farwell	(601) 688-4875	NOARL 242

DD Form 1473, JUN 86 Previous editions are obsolete

SECURITY CLASSIFICATION OF THIS PAGE

S/N 0102-LF-014-6603

UNCLASSIFIED

Distribution List for APL-UW TR 8815

Assistant Secretary of the Navy
(Research, Engineering and Systems)
Department of the Navy
Washington, DC 20350 [2 cp]

Chief of Naval Operations
Department of the Navy
Washington, DC 20350-2000

OP 02
OP 22
OP 223
OP 225
OP 07
OP 071
OP 095
OP 96T
OP 0962E
OP 0962X
OP 098

Director of Defense Research
Office of Assistant Director (Ocean Control)
The Pentagon
Washington, DC 20301-5000

Defense Technical Information Center
Cameron Building #5
Alexandria, VA 22304-6145

Office of Naval Research
Department of the Navy
800 N. Quincy Street
Arlington, VA 22217-5000

ONR 00
ONR 000A
ONR 112
ONR 1125
ONR 1125AR
ONR 1125OA
ONR 1222T
ONR 124 [2 cp]
ONR 22
ONR 23
ONR 23D
ONR 232
ONR 234

Office of Naval Research
R. Silverman, Resident Representative
315 University District Bldg., JD-16
1107 N.E. 45th Street
Seattle, WA 98195

Director
Defense Advanced Research Projects Agency
1400 Wilson Boulevard
Arlington, VA 22209

Commanding Officer
Naval Intelligence Support Center
4301 Suitland Road
Washington, DC 20390

Commanding Officer
Naval Polar Oceanographic Center
4301 Suitland Road
Washington, DC 20390-5140

Library

Center for Naval Analyses
4401 Ford Avenue
P.O. Box 16268
Alexandria, VA 22302-0268

Attn: Technical Information Center

Commander
Naval Air Systems Command Hq.
Department of the Navy
Washington, DC 20361

AIR 340L

Commander
Space and Naval Warfare Systems Command (NC1)
(SPAWAR)
Department of the Navy
Washington, DC 20363-5100

SPAWAR 005
PMW-180
PMW-181
PMW-182
PMW-182-2

Commander
Naval Sea Systems Command
Department of the Navy
Washington, DC 20362

NSEA 05R
NSEA 06
NSEA 06UB
NSEA 63D [2 cp]
NSEA 63D4
Code PMS-402
Code PMS-406
Code PMS-407 [2 cp]

Commanding Officer
Naval Underwater Systems Center
Newport, RI 02840

Library [2 cp]
Code 00
Code 22202
Code 3824
Code 801
Code 81
Code 8211 [2 cp]
Code 8212

Officer-in-Charge
New London Laboratory
Naval Underwater Systems Center
New London, CT 06320

Library
Code 01Y [2 cp]
Code 2111
Code 3423

Commander
Naval Weapons Center
China Lake, CA 93555

Library

Commander
Naval Ocean Systems Center
San Diego, CA 92152-5000

Library
Code 00
Code 19 [3 cp]
Code 541
Code 844 [3 cp]

Commanding Officer
Naval Coastal Systems Center
Panama City, FL 32407

Library

Commander
Naval Surface Warfare Center
White Oak
Silver Spring, MD 20903-5000

Library [2 cp]
Code R-01
Code R-43 [2 cp]
Code U-04
Code U-06
Code U-42 [2 cp]

Commanding Officer
Naval Civil Engineering Laboratory
Port Hueneme, CA 93043-5003

Library
Code L14
Code L43 [2 cp]

Director
Naval Research Laboratory
Washington, DC 20375

Library
Code 5100
Code 5123

Commanding Officer
Naval Oceanographic and Atmospheric
Research Laboratory
Stennis Space Center, MS 39529-5004

Library [2 cp]
Code 113
Code 200
Code 210
Code 240
Code 242 [3 cp]
Code 252

Commanding Officer
Naval Oceanographic Office
Stennis Space Center, MS 39522-5001

Code OA
Code OAR
Code OARU

Commander
Naval Air Development Center
Warminster, PA 18974

Library
Code 3031 (A. Horbach)

Commander
David Taylor Research Center
Bethesda, MD 20084

Library
Code 1720 [2 cp]
Code 1908

Commanding Officer
Naval Submarine School
Box 70
Naval Submarine Base -- New London
Groton, CT 06340

Superintendent
Naval Postgraduate School
Monterey, CA 93943-5100

Library [2 cp]
Code 68

Commander, SECOND Fleet
Fleet Post Office
New York, NY 09501

Commander, THIRD Fleet
Fleet Post Office
San Francisco, CA 96601

Commander Submarine Force
U.S. Atlantic Fleet
Norfolk, VA 23511

Code 00
Code 019
Code 22
Code N311

Commander Submarine Force
U.S. Pacific Fleet
Pearl Harbor, HI 96860

Code 00
Code N2
Code N21

Commander
Submarine Squadron THREE
Fleet Station Post Office
San Diego, CA 92132

Commander
Submarine Group FIVE
Fleet Station Post Office
San Diego, CA 92132

Commander
Submarine Development Squadron TWELVE
Box 70
Naval Submarine Base - New London
Groton, CT 06340

Code 20

Knut Aagaard
Pacific Marine Environmental Laboratory
NOAA
7600 Sand Point Way NE, Building 3
Bin C15700
Seattle, WA 98115-0070

Director
Applied Research Laboratories
The University of Texas at Austin
P.O. Box 8029
Austin, TX 78713-8029

Library
N. Bedford
M. Lawrence
T. Lawrence

Director
Applied Research Laboratory
The Pennsylvania State University
State College, PA 16801

C. Ackerman
R. Ingram [2 cp]
E. Liszka
S. McDaniel
F. Symons, Jr.
D. Upshaw
F. Reeser

Polar Research Laboratory, Inc.
6309 Carpenteria Avenue
Carpenteria, CA 90813

Sandia National Laboratories
Kirtland Air Force Base
P.O. Box 5800
Albuquerque, NM 87185

Commander, British Naval Staff
P.O. Box 4855
Washington, D.C. 20008
Attn: CDR A.M. Poulter [2 cp]

Library